https://doi.org/10.1016/j.engstruct.2021.112692

Chord plastification in high strength steel circular hollow section X-joints: testing, modelling and strength predictions

Yancheng CAI, Tak-Ming CHAN * and Ben YOUNG

Department of Civil and Environmental Engineering, The Hong Kong Polytechnic University, Hong Kong

Abstract

This paper presents experimental and numerical investigations on cold-formed high strength steel (CFHSS) circular hollow section (CHS) X-joints. The CFHSS CHS members had nominal 0.2% proof stress up to 1100 MPa. The geometric parameters of the X-joints were designed by varying the ratios of β, 2γ and τ. Seventeen X-joint tests were conducted by applying axial compressive load through the braces without preloading in chords. Non-linear finite element model (FEM) was then developed for the CFHSS CHS X-joints. After successful validation of ultimate strengths, failure modes and load-deformation curves, parametric studies were performed by using the verified FEM. The chord plastification failure of the X-joints was mainly found in both test and numerical studies. The relationship between the joint strengths and the variation of geometric ratios were investigated. The strengths of the X-joints obtained in this study together with the test strengths collected from the literature were used to assess the strength predictions by CIDECT and EN-1993-1-8, as well as those from the literature. It was found that the current predictions generally provided unconservative predictions. A new equation that considers the effects of geometric ratios on the strengths was proposed based on both the test and numerical results. By adopting the newly proposed equation, the predictions are improved and provide the least scattered results when compared with the other predictions.

Key words: Cold-formed high strength steel; chord plastification; circular hollow section; experimental investigation; numerical investigation; tubular X-joints.

* Corresponding author.
E-mail address: tak-ming.chan@polyu.edu.hk

1. Introduction

With the advancements in material and fabrication techniques, steel tubular members with higher strength have been produced in different section profiles. Nowadays, steel tubular members with yield strength (0.2% proof stress) over 1000 MPa are available in the market. The application of higher strength steel tubular members can reduce dimensions and numbers of members in steel structures, reducing the overall weight of the structure with the associated reductions in transportation, handling, erection time and costs of foundation [1]. These advantages are favoured by architects, engineers and developers. However, the current international steel design specifications [2-4] are applicable for structural steel with yield strength (0.2% proof stress) up to 700 MPa, for example, the European Code EN 1993-1-12 [2]. This gap in terms of steel grades between the market and design specifications has driven the investigations on high strength steel (nominal yield strength not less than 690 MPa) in material properties [5-11], beams subjected to three-point bending and/or four-point bending [12-15], columns subjected to axial compression and/or combined axial compression and bending [16-25] as well as bolted connections [26-33] and welded joints [34-42] in the last decade. Furthermore, the high strength steel tubular members were also investigated in composite structures, such as concrete-filled steel tubular columns [43-44]. Appropriate design rules have been proposed to overcome the shortage of the current steel design specifications, such as design of beams subjected to bending [13,15], columns under axial compression [18-20] as well as combined compression and bending [22], and tubular T-joints [41]. The fatigue of high strength steel is also an important issue due to the increased strength and reduced material ductility when compared with conventional strength steel.

Welded steel tubular joints are widely used in onshore and offshore structures. Design guides for tubular joints under different loading conditions have been developed based on extensive research projects on steel tubular structures. These research projects were mainly conducted under the direction

of Comité International pour le Développement et l'Etude de la Construction Tubulaire (CIDECT) and International Institute of Welding (IIW) Sub-commission XV-E [45-46]. The IIW published its first edition of design recommendations on static strength of steel tubular joints [47] in 1981, the second edition [48] in 1989 and then the third edition [49] in 2009. At the same period, the CIDECT provided its first edition of the design guides for circular hollow section (CHS) joints [50] in 1991 and rectangular hollow section (RHS) joints [51] in 1992; and the second edition for CHS joints [52] in 2008 and RHS joints [53] in 2009. These design guidelines [47-53] are applicable for steel tubular joints under predominantly static loading. The design recommendations proposed by IIW and CIDECT have been adopted by many international standards [3,4, 54-56] around the world. These designs are generally valid for both cold-formed and hot-finished steel members with nominal 0.2% proof stress (yield strength) not exceeding 460 MPa and nominal wall thickness in the range from 2.5 mm to 25.0 mm, as discussed by Tong and Zhao [46]. The emerged higher strength steel tubular members are not covered by these design guidelines. Hence, these design guidelines may not cater for the needs in the safe and reliable design of tubular joints in steel structures.

In terms of the effects on strength of welded steel tubular joints due to the higher steel grades utilised, the current version (2nd Version) of CIDECT [52,53], as compared to its first edition [50,51] for steel grade up to S355 (having nominal yield strength of 355 MPa), extended the steel grade up to S460 (having nominal yield strength of 460 MPa) by limiting the design yield strength (0.2% proof stress, $f_{0.2}$) not higher than 0.8 times the ultimate strength ($0.8f_u$), and imposing a further reduction factor of 0.9 in the design. Likewise, a reduction factor of 0.9 is specified in EN 1993-1-8 [55] to enable the design equation applicable to steel grades exceeding S355 but limited to S460. The EN 1993-1-12 [2] further extended the design to steel grade up to S700 by multiplying another reduction of 0.8. These reduction factors are imposed mainly for the consideration of possibly lower rotation and deformation capacity as

well as for the required sufficient ductility [52,53]. The suitability of these design rules with reduction factors for high strength steel tubular joints are controversial [41], for example, the recent numerical investigations on high strength steel (nominal yield strength up to 1100 MPa) CHS X-joints by Lan *et al.* [38] showed that the strength predictions by CIDECT [52] and EN-1993-1-8 [55] became increasingly unconservative as steel yield strength increased.

Design rules for welded CHS X-joints (both brace and chord members) were developed mainly based on the analytical model firstly proposed by Togo [57]. The proposed model indicates that the chord plastification strength of the joints subjected to axial loading in braces is the function of the yield strength together with the square of chord wall thickness (t_0). Based on this principle, design equations for CHS X-joints were developed by carrying out extensive experimental and numerical investigations, where the key geometric parameters were considered in the equations including the ratios of brace outer diameter (d_1) to chord outer diameter (d_0) in $\beta = d_1/d_0$, the d_0 to chord wall thickness (t_0) ratio in $2\gamma = d_0/t_0$ as well as brace wall thickness (t_1) to the t_0 in $\tau = t_1/t_0$. With the shortcomings of the current design guidelines along with the rapid development in high strength steel tubular members as discussed earlier, the purposes of this study are to investigate the effects of the key geometric parameters on the chord plastification strengths of cold-formed high strength steel (CFHSS) CHS X-joints by experimental testing and numerical modelling; and to assess the applicability of the existing design guidelines for the CFHSS CHS X-joints with nominal 0.2% proof stress up to 1100 MPa. The CFHSS X-joints were loaded by axial compressive force in braces without chord preloading. Finally, a new design equation is derived for the strength prediction of CFHSS CHS X-joints failed by chord plastification (chord face failure), based on the test and numerical results obtained in this study and the test results in literature.

2. Experimental investigation

2.1 *Design of test specimens*

A series of CFHSS CHS X-joint (see Figure 1) tests was conducted in this study. The CFHSS members had the nominal 0.2% proof stress ($f_{0.2,n}$) up to 1100 MPa, and five different sections ($D \times t$ in millimetre) with the nominal outer diameter (D) and thickness (t) of 22×4, 55×11, 89×4, 108×4 and 133×4. The sections of 89×4, 108×4 and 133×4 were used as the chord members of the X-joints. The nominal section size that had outer diameter smaller than or equal to that of the chord member was paired as the brace member. In the design of test specimens, the geometric parameters that are related to the resistance of CHS X-joints were considered, namely, the ratios of β ($\beta = d_1/d_0$), 2γ ($2\gamma = d_0/t_0$) and τ ($\tau = t_1/t_0$). The t_1 is the brace wall thickness. It should be noted that the section of 89×4 had the $f_{0.2,n}$ of 900 MPa and 1100 MPa, as distinguished by 89×4^ and 89×4*, respectively, in the content of this paper. Hence, four series of X-joints were designed based on the selection of chord members (i.e., the 89×4^, 89×4*, 108×4 and 133×4), as shown in Table 1. The specimens were generally identified by two segments, namely, segment of the brace section followed by that of the chord section (brace - chord). If it was a repeated test specimen, it was indicated by -r in the labelling.

The nominal chord length (l_0) was taken as the sum of the brace outer diameter (d_1) and 4.0~5.0 times chord outer diameter (d_0). The value of $l_0 = 6d_0$ was adopted by Lan *et al.* [58] for high strength steel CHS X-joints, while $l_0 = d_1 + 4d_0$ was adopted by Pandey and Young [42] for high strength steel tubular X-joints. In this investigation, the design principle of l_0 was considered that the adequate load distribution in the chord member was achieved and the stresses at the brace and chord intersection were not affected by the chord ends, as illustrated in the numerical analysis in this study. The chord length of the X-joint specimens in this study satisfied the minimum member length ($d_1 + 3d_0$) for the Interior-One-Flange (IOF) loading case of web crippling tests specified in NAS [59]. The nominal brace length (l_1)

was designed as $2d_1$ that measured from the crown of the chord to the brace end [42,58]. It should be noted that the chord and brace tubes were fabricated by press-braked and cold-rolled, respectively, for the high strength steel CHS X-joints tested by Lan *et al*. [58]. The tubes were fabricated from one Chinese Q960 steel plate with a nominal yield stress of 960 MPa [58]. In the present study, the tubes of 22×4 and 55×11 were hot-rolled seamless sections, while the tubes of 89×4, 108×4 and 133×4 were cold-formed circular hollow sections.

In all the CFHSS CHS X-joint specimens, the chord member was oriented such the weld seam of the section was at 90 degree away from the top of the chord (see Figure 1). The weld seam of the brace member was oriented at 90 degree from the longitudinal direction of the chord member. The brace member was wire-cut at both ends with one end flat and another end fitting the profile of the paired chord [60]. The dimensions of each CFHSS CHS X-joint specimen were measured and the average values for each dimension are tabulated in Table 1. The geometric ratios of β, τ and 2γ were calculated from the measurements. The smaller measured values of the upper and lower braces were used in the determination of β and τ ratios. In summary, the β, τ and 2γ of the test specimens varied from 0.17 to 1.00, from 0.96 to 2.77 and from 22.50 to 34.22, respectively.

2.2 *Welding and material properties*

A robotic gas metal arc welding (GMAW) was employed in the welding between brace and chord of the CFHSS CHS X-joints, which is the same as those used for CFHSS tubular joins in [40,42]. The AWS D1.1M Specification [61] was followed in the fabrication of the X-joints. A low alloy carbon steel wire with a diameter of 1.2 mm was used as a filler material. It conformed to Class ER120S-G of the AWS A5.28M Specification [62]. The $f_{0.2,n}$, nominal tensile strength ($f_{u,n}$) and elongation of the steel wire were 930 MPa, 980 MPa and 19%, respectively [40,42]. The sizes of weld legs (see Δ_1 and Δ_2 in Figure 2(a)) in the X-joint specimens were greater than the minimum value specified in the AWS D1.1M

Specification [61]. This minimum value is set as the maximum of $1.5t_{min}$ or 3 mm, where t_{min} is the thickness of the thinner tube. The welding throat thickness (Δ_3) of the specimens was also measured, as illustrated in Figure 3. The welding details at the joint saddle for those specimens with β = 1.0 were illustrated in Figure 2(b). The average measured values of the CHS X-joint specimens are also tabulated in Table 2.

Tensile coupon tests were conducted to obtain the material properties of the CHS. The coupons were machined from the centre of the face at 90˚ from the seam weld in the CFHSS tubes, which represented the crown location at the chord of the X-joints (see Figure 1). The dimension of the coupon specimens had 4 mm width and 25 mm gauge length. The specimens were tested between two pins through specially designed grips such that tension load was applied through the centroid of the coupon [8]. Two strain gauges were used to measure the initial Young's modulus of the material, while an extensometer was used to obtain the rest of the stress-strain curve until fracture. The material properties that based on the 25 mm gauge length of the coupon specimen were obtained, including the modulus of elasticity (E), the measured static 0.01% proof stress ($f_{0.01}$), $f_{0.2}$ and tensile strength (f_u), strain at tensile strength (ε_u) and fracture failure (ε_f), as shown in Table 3. The Ramberg-Osgood parameter (n) was calculated according to $n = ln(0.2/0.01)/\ln(f_{0.2}/f_{0.01})$.

2.3 *Test rig and* procedure

The CFHSS CHS X-joints were tested in a servo-controlled hydraulic testing machine. The photo of test setup for specimen 89×4* - 108×4 is shown in Figure 4. The bottom end of the lower brace was placed on a hardened high strength steel bearing plate with flat surface. A special ball bearing head was used at the top of the testing machine. The ball bearing can be self-adjusted to fully contact the top end of the upper brace by applying a small loading. After concentrically positioning the X-joint with alignments checking, the actuator ram of the testing machine was slowly moved up until an axial load

of around 4.0 kN was applied on the specimen. The X-joint specimen was preloaded. This process enabled the free-rotated ball bearing to fully contact the upper brace end. Any gaps in the specimen and steel bearing plates were eliminated. After the preloading process, the position of the ball bearing was locked from any rotations in the rest of the test.

The local deformations of the CFHSS X-joint specimens were carefully measured by the calibrated linear variable displacement transducers (LVDTs), as illustrated in Figure 5. The chord face indentations of the specimen were measured at the chord crown on each side of the brace by the 4 LVDTs, namely the No.1~4 shown in Figure 5(a). The extension arms were attached to the tips of the respective LVDTs such that the position next to the welding closest to the adjacent brace face was measured, i.e., around 6.0 mm from the adjacent brace face. (Note that the welding length of Δ_1 is around 6.0 mm as shown in Table 2). Two horizontal LVDTs (No.5 and No.6 shown in Figure 5(b)) were used to measure chord horizontal deflections at the middle of the chord. Their tips were assembled with Poly Methyl Methacrylate (PMMA) plates (see Figure 4) to ensure the chord horizontal deformations were captured during testing. Hence, the maximum chord horizontal deformations could be fully captured. In addition, two vertical LVDTs (No.7 and No.8 shown in Figure 5(a)) were used to record the overall axial displacement of the actuator ram throughout the test.

Displacement control mode was adopted in the tests of CFHSS CHS X-joints. A constant loading rate of 0.3 mm/min was adopted throughout the tests. The tests were generally paused for 90 s at two moments, namely near the ultimate loads and at post ultimate loads. The static drops were obtained from the pauses; hence the effects of loading rates could be isolated from the test strengths. The tests did not stop until a clear drop of loading was observed. A data acquisition system was used to record the applied load and the LVDTs readings during the tests.

2.4 *Test results*

The test results of the CFHSS CHS X-joints are summarized in Table 4. The test strengths were determined from the static load-deformation curves. The static load-deformation curves were obtained from the static drops as mentioned earlier. All the specimens experienced a clear ultimate load (peak load) in the load-deformation curves and failed by chord plastification (chord face failure). The ultimate load (P_u) and the corresponding axial shortening (μ_u) at one side (half of the average readings from LVDTs Nos.7&8) were tabulated in Table 4. In addition, the load ($P_{3\%}$) corresponding to the axial shortening of $\mu_{0.03}$ ($\mu_{0.03} = 0.03d_0$) at one side was also obtained from the test curve and shown in Table 4. However, the values of μ_u and $\mu_{0.03}$ were obtained based on half of the average readings of the two LVDTs (i.e., Nos.7&8). The measurements obtained from the 4 LVDTs (i.e., Nos.1~4) were not used. This is because that slight tilting of the chords (from the crown of the joint to the chord end) was observed due to the relatively large chord indentation in the tests. This affected the accurate measurements of the 4 LVDTs that were positioned at the chord ends. The major axial deformation of the X-joints was due to the indentation of the chords. Figures 6(a) and 7(a) illustrate the applied load versus the chord side wall deformation curves, for specimens with chords of 133×4 and 108×4, respectively. The chord side wall deformations were obtained by the average values from LVDTs of Nos.5&6. The corresponding loads versus the measured axial shortenings (half of the average values from LVDTs of Nos.7&8) were shown in Figures 6(b) and 7(b). The chord deformation of specimen 89×4^ - 108×4 during test is illustrated in Figure 8(a).

3. Numerical investigation

3.1 *General*

The finite element model (FEM) using the ABAQUS program of version 6.20 [63] was developed to simulate the tests of axial loaded CFHSS CHS X-joint specimens. The FEM was validated by the comparisons of strengths, failure modes and load-deformation curves between the numerical results and

test results. After successful validation, extensive parametric studies by using the FEM were performed.

3.2 *Development of FEM and validation*

The measured specimen dimensions (see Table 1) were used in the development of X-joints in FEM. The shell element type S4R was selected to simulate the brace member and chord member of the CHS X-joints. The previous study by Lan *et al*. [37] showed that the differences of the finite element analysis (FEA) results were comparable with a maximum deviation of 5%, when comparing the results from FEM using S4R element without considering weld detail and those using solid element type C3D8R with considering weld detail in CHS X-joints. In their analysis, the specimens with the maximum chord diameter of 244.7 mm and thickness of 22.0 mm tested by Puthli *et al*. [35] were used. Hence, in this study, the weld detail of the X-joint specimens was not considered. A more recent study by Lan *et al*. [38] found that the effects of reduced material properties in heat affected zones (HAZ) on the strengths of CFHSS CHS X-joints was relatively insignificant, as the stress in the HAZ could be effectively redistributed to the adjacent areas of base metals. In addition, it was explained that the improved yield strength of steel in CHS X-joints was generally under-utilised due to the adopted indentation limit [38], which will also be illustrated in the curves of the parametric studies in this paper. The effect of steel material properties due to HAZ in the weld region was thus not modelled in the FEM. The finer mesh sizes were adopted in the weld region with a length of d_0 from the centre line of the joint to the chord end or brace end (see Figure 8(b)); however, coarse elements were used for the rest parts of the X-joints [37-38].

The engineering stress-strain (σ-ε) curves obtained from the coupon tests were converted to true stress (σ_{true}) and logarithmic plastic strain (ε_{true}^{pl}) curves by following Equations (1)-(2):

$$\sigma_{true} = \sigma\,(1 + \varepsilon) \tag{1}$$

$$\varepsilon_{true}^{pl} = ln(1 + \varepsilon) - \frac{\sigma_{true}}{E_s} \tag{2}$$

The converted true stress-true plastic strain curves were assigned to the corresponding braces and chords in the FEM. The boundary conditions of the X-joints were simulated according to the conditions in the tests. Two reference points (RP1 at the end of upper brace and RP2 at the end of lower brace) were defined at the brace ends (see Figure 9). They were fully coupled with the respective brace end surfaces. Hence, the RP1 and RP2 were restricted in all degrees of freedom, except for the axial displacement of the RP1. The geometrical nonlinearity (*NLGEOM) was activated in the FEM to consider the large deformation of the X-joint. The reference points of RP3 and RP4 (see Figure 9) were defined in the crowns of the chord, with 6 mm away from the outer surfaces of the upper brace and lower brace to monitor the chord face indentation. The reference point of RP5 was defined at middle of the chord surface to monitor the horizontal deformation of the X-joint, as shown in Figure 9. The loads were applied by specifying axial displacements to the RP1 of the FEM, which was identical to the test programme by displacement control test method. Static analysis method was used in performing the FEA.

All the specimens from the FEA failed by chord plastification, the same failure mode as those of the test specimens. The strengths obtained from the FEA, namely the strength ($P_{FE\text{-}1}$) corresponding to the $\mu_{0.03}$ which was based on half value of the axial shortening as those defined from the tests. and the ultimate strength ($P_{FE\text{-}u}$) were shown in Table 4. The test strengths were compared with the FEA strengths by $P_{3\%}/P_{FE\text{-}1}$ and $P_u/P_{FE\text{-}u}$. The mean values of $P_{3\%}/P_{FE\text{-}1}$ and $P_u/P_{FE\text{-}u}$ were 0.98 and 0.95 with the corresponding coefficient of variation (COV) of 0.062 and 0.070. Figure 8(a) illustrates the comparison of failure mode between test and FEA for specimen 89×4^-108×4. The elevation view of the specimen failure and the stress contour are shown in Figure 8(b). Generally, the higher stresses (reaching yield stress) were found within the length of $1.0d_0$ from the centreline of the joint. Similar findings were illustrated in Lan *et al.* [37,38]. Figures 10(a)-(b) further illustrate the comparison of load

versus the deformation curves of the CFHSS CHS X-joints between the test and FEA results. Half displacement of RF1 and the total deformation of RF5 were used in plotting the axial shortening and chord horizontal deformation curves, respectively. Overall, it is shown that the developed FEM could replicate the tests of CFHSS CHS X-joints in terms of joint strengths, failure mode and histories of applied load versus deformations. The results obtained from RP3 and RP4 will be used to determine the chord indentation and the corresponding joint strength of test specimens in the later analysis of this study.

3.3 *Parametric studies*

After successful validation of the FEM, the FEM was used to perform the parametric studies for the structural performance of CFHSS CHS X-joints subject to axial compression in braces. The geometric parameters of the CHS X-joint design equations [52,55] were considered, and their interactions were reflected in the parameters of the β, τ and 2γ. The length of the braces was taken as $2d_1$ and that of the chords was taken as ($d_1 + 5d_o$). Same as those test specimens, the chord members of the CFHSS CHS X-joints in the parametric studies were not preloaded.

The designed X-joints for the parametric studies are summarized in Table 5. In the joint designs, three different chord members based on the commonly used steel product catalogue were selected to represent the relatively small, medium and large sizes of CHS members, with the dimensions ($D \times t$ in millimetre) of 88.9×6.3, 273×12.5 and 508×12.5, respectively. Hence, there are three series of X-joints in terms of chord outer diameter variations (d_o) as represented by Series A, B and C in the content of this paper. In each series, the geometric parameters of the joints were determined based on the predetermined values of β, τ and 2γ. The values of β, τ and 2γ were mainly set as 0.40, 1.00 and 14.11 in Series A. In Series A, the effects of β, τ and 2γ on the joint behaviour were studied by verifying one factor while maintaining the other two factors the same (see Table 5). Hence, the cross-sectional dimensions of the brace and chord members were then determined. By using the same principle, the values of β, τ and 2γ

were mainly set as 0.60, 0.60 and 21.84 & 0.80, 0.40 and 40.64 for Series B and C, respectively. Same labelling system was adopted as that for the test specimens. Details of the specimens with the geometric ratios are shown in Tables 6-8, for Series A, B and C, respectively.

The material properties of section 108×4 (see Table 1) obtained from the coupon tests were used in the parametric studies. In total, 75 parametric results were generated for the CFHSS CHS X-joints subjected to axial loading in braces. All these 75 X-joints mainly failed by chord plastification. In each series, the curves of load versus the chord side wall deformation and those of load versus the chord indentation are plotted, as shown in Figures 11-13 for specimens Series A, and in Figures 14-16 for Series B and Figures 17-19 for Series C. The chord face indentation (μ) was obtained by half of the difference in axial displacements of RP3 and RP4, i.e., ($|\Delta_{RP3}| - |\Delta_{RP4}|$)/2. In the figure of each series, the value of chord face indentation equal to 3%d_0 was identified. The strengths ($P_{FE\text{-}0.03}$) of the X-joints corresponding to chord face indentation of 3%d_0 were obtained. It should be noted that six specimens did not reach the chord face indentation value of 3%d_0 due to the premature of brace local buckling. These specimens were marked by $^{\#}$, as shown in Tables 6-8, and they were not used in the further analysis. Some specimens experienced chord face indentation of 3%d_0 but still not reached the peak strength although they were axially loaded with total end shortening of over 50 mm, particularly for those of Series C (see Figures 17-19). Hence, the strengths (P_{FE}) of the X-joints in parametric studies were determined by $P_{FE} = P_{FE\text{-}u}$ if $\mu_p \leq 3\%d_0$; otherwise, $P_{FE} = P_{EF\text{-}0.03}$ if $\mu_p > 3\%d_0$. $P_{EF\text{-}u}$ and μ_p are the ultimate (peak) strengths and the corresponding chord face indentation of an X-joint. Same strength definitions with respect to 3%d_0 have been widely adopted for CHS X-joints in the literature [36-38]. The strengths (P_{FE}) of the X-joints in parametric studies are tabulated in Tables 6-8.

4. Structural performance

4.1 *Deformation capacity and ductility*

The current design guidelines are generally strength-based, but without specifying any requirements for the deformation capacity and ductility of steel tubular joints [58], including those in this study. The chord face indentation limit of 3%d_0 for steel CHS X-joints was firstly suggested by Lu *et al.* [64], as they found that for the steel tubular joints exhibiting peak loads generally had the chord face indentations within 2.5%d_0 ~ 4%d_0 in the load-deformation curves. Hence, the chord face indentation limit of 3%d_0 was proposed for the steel tubular X-joints without exhibiting peak loads because of material strain hardening and membrane action. It should be noted that such limit was based on steel tubular joints made up of normal strength steel, but not high strength steel. However, the recent experimental investigation on six CFHSS CHS X-joints with $f_{0.2}/f_u$ ranging from 0.87 to 0.91 and ε_f ranging from 13.5% to 17.8% in chord members, as well as values of the β ranging from 0.60 to 0.93, showed that the deformation capacity of the joints could be considered as reasonably sufficient, as evidenced by the indentations at peak loads that were generally at least twice of the respective values of 3%d_0 [58].

The ductility of CFHSS members in the X-joint specimens is also relatively low with the yield ratio ($f_{0.2}/f_u$) of around 0.90 and the fracture strain (ε_f) around 11.0% (see Table 3). However, as also found by Lan *et al*. [58], it is shown that all testing curves exhibited similar slow-descending without sudden drop of loads after reaching the peak loads (see the test curves of the present study in Figures 6-7). Similar findings were shown in the curves (see Figures 11-19) that were obtained from the parametric studies of this paper, except for those failed by brace local buckling. For the X-joints with chords members of medium and large sizes (d_0 = 273 and 508 mm), almost all the curves had not reached the peak loads after experiencing the chord face indentation of 0.03d_0. Larger deformation capacity of these specimens could be anticipated from the figures. Hence, this is favourable for the application of the CFHSS CHS X-joints when the issue of joint deformation and ductility was a concern. Note that this study mainly focusses on the X-joint specimens that failed by chord plastification without preloading in the chords.

4.2 *The effects of geometric parameters*

The effects of geometric parameters on the strengths of CFHSS CHS X-joints failed by chord plastification were analysed. In the investigation of the effects due to the variations of β in each sub-series, the strengths (P_{FE}) were normalized by the strength corresponding to β = 0.9. By following this, the strengths (P_{FE}) in the sub-series were normalized by 817.2 kN in Table 6 for τ = 1.00 and 2γ = 21.84, and by 3201.3 kN in Table 7 for τ = 0.60 and 2γ = 21.84 and by 2978.2 kN in Table 8 for τ = 0.40 and 2γ = 40.64. Similarly, in the investigation of the effects due to the variations of τ in each sub-series, the strengths (P_{FE}) were normalized by the strength corresponding to τ = 0.9. For those due to the variations of 2γ in each sub-series, the values of P_{FE} were normalized by the strength corresponding to around 2γ = 20. The normalized values for each sub-series are shown in the last columns of Tables 6-8.

The effects of β, τ and 2γ on the joint strengths are plotted in Figures 20-22, respectively. In each figure, the results of the three sub-series from Series A, B and C were used. As shown Figure 20, the X-joint strengths increased as the value of β increased, and the increments were larger as the β became larger regardless of different sets of τ and 2γ. Furthermore, for each set of τ and 2γ, the trend of strength increments with increasing of β was similar with each other. However, the variation of τ had little effects on the strength of the X-joints for different sets of β and 2γ (see Figure 21). On the contrary to those findings in the effects due to β, the X-joint strengths decreased as the value of 2γ increased, and the decrements were smaller as the 2γ became larger regardless of different sets of β and τ. For each set of β and τ, the trend of strength decrements with decreasing of 2γ was similar with each other.

5. Strength prediction of existing design rules

5.1 *Design guidelines*

As discussed in Section 1 of this paper, the strength (P) for steel CHS X-joints that failed by chord plastification is function of the 0.2% proof stress (yield strength) together with the square of chord wall

thickness ($f_{0.2}t_0^2$) based on the analytical model proposed by Togo in 1967 [57]. The design formulas were developed based on this principle by considering the effects due to the geometrical parameters as represented by Q_u and the preloading condition of the chord by Q_f, which is shown in Equation (3). The angle (θ) between the brace and chord is considered by $sin\theta$, which is equal to 1.0 for all the X-joints in this study. The Q_u and Q_f were determined using multi-regression analyses of the experimental and numerical results. The development of the design equations in the CIDECT and IIW were discussed in detail by Zhao *et al*. [45] and Zhao and Tong [46].

$$P = Q_f Q_u \frac{f_{0.2} t_0^2}{\sin\theta} \quad (3)$$

The CFHSS CHS X-joints in this study were designed without any preloading in the chords. Hence, the Q_f is equal to 1.0. The determination of Q_u is related to the geometric parameters such as β, τ and 2γ, and generally represented by Equation (4), where *A*, *B*, *and C* are regression coefficients. The parameter of τ is not considered in Equation (4) as it has limited effect on the joint strengths that failed by chord plastification, which is also illustrated in Figure 21 of this paper.

$$Q_u = \left(\frac{A}{1-B\beta}\right)(\gamma)^C \quad (4)$$

The design guide in CIDECT [52] is generally based on the 3rd edition of the IIW recommendations [49]. It updates the strength equations by considering the chord indentation limit of 3%d_0. Background of the 3rd edition of IIW recommendations [49] is explained by van der Vegte *et al*. [65]. The determination of Q_u in CIDECT [52] is shown in Equation (5), as represented by $Q_{CDT,f}$.

$$Q_{CDT,f} = 2.6\left(\frac{1+\beta}{1-0.7\beta}\right)\gamma^{0.15} \quad (5)$$

The Equations (3) and (5) provided factored strength of steel CHS X-joints. This is because a safety factor equal to 1.22 has been included [58]. Hence, the nominal strength (unfactored) of X-joints should be determined by Equations (3) and (6).

$$Q_{CDT,n} = 3.16\left(\frac{1+\beta}{1-0.7\beta}\right)\gamma^{0.15} \quad (6)$$

The validity ranges of the Equation (6) for the steel CHS X-joints are $0.2 \leq \beta \leq 1.0$, $2\gamma \leq 40$ and $\theta \geq 30°$. All the CFHSS CHS X-joints in this study had the same $\theta = 90°$, with $0.2 \leq \beta \leq 1.0$, $0.2 \leq \tau \leq 1.0$ and $10.0 \leq 2\gamma \leq 50.0$. The nominal strength calculations in this study, the reduction factor of 0.9 together with the material strength in the minimum of $f_{0.2}$ and $0.8f_u$ were used, as previous numerical studies showed that the predictions overestimated the test strengths for high strength steel CHS X-joints [37].

The Q_u for steel CHS X-joints in EN 1993-1-8 [55] is, however, mainly based on the 2nd edition of the IIW recommendations [48], which takes the peak loads as the joint strengths. The determination of $Q_{EC,f}$ as specified in Table 7.2 of EN 1993-1-8 [55] is re-written in Equation (7) as shown below:

$$Q_{EC,f} = \frac{5.2}{1-0.81\beta} \quad (7)$$

A partial safety factor (γ_{M5}) equal to 1.0 is suggested for the resistance design in EN 1993-1-8 [55]. This is because Equation (7) has implicitly adopted a safety factor of 1.28. In this sense, the nominal strength of steel CHS X-joints predicted by EN 1993-1-8 [55] should be calculated by Equation (3) together with the nominal $Q_{EC,n}$ as determined by Equation (8).

$$Q_{EC,n} = \frac{6.67}{1-0.81\beta} \quad (8)$$

The parameter of γ is not shown in Equations (7) and (8). This is because they were developed based on the original Equation (9) in Wardernier [66].

$$Q_W = \frac{7.46}{1-0.812\beta}(2\gamma)^{-0.05}(f_{0.2}/f_u)^{-0.173} \quad (9)$$

The Equation (9) is simplified by adopting $2\gamma = 40$ and $f_{0.2}/f_u = 0.66$ as it was found that the strengths of the investigated X-joints were less sensitive under the variations of γ and $f_{0.2}/f_u$ in Equation (9) [66]. The Equation (8) is applicable for steel CHS X-joints in the ranges of $0.2 \leq \beta \leq 1.0$, $10.0 \leq 2\gamma \leq 50.0$ and $\theta \geq 30°$, as specified in EN 1993-1-8 [55]. The reduction factor of 0.9 is specified [55] for steel with

nominal yield strength exceeding 355 MPa and a further reduction factor of 0.8 is specified [2] for steel with nominal yield strength greater than 460 MPa up to 700 MPa. Hence, these two factors were used in the nominal strength calculations in this study. In addition, to make a direct comparison, the predictions by using Equation (9) were also assessed in this study, however, the reduction factors were not used for Equation (9).

It should be noted that for the above equations, the brace cross sections of the X-joints are required to be Class 1 or 2 to avoid premature of brace local buckling. In this study, the X-joints that failed by brace local buckling before reaching the chord face indentation of 3%d_0 or ultimate load were excluded from the analysis regardless of the brace cross section classifications. The X-joints that failed by chord plastification having chord face indentation of not less than 3%d_0 or reaching clear peak load before such indentation were used to assess the design equations regardless of cross section classifications of the braces. Those 6 specimens (see Tables 6-8) that failed by local buckling of the braces in the X-joints were not included in the analysis in this paper.

5.2 *Design equation proposed by Lan et al. [38]*

Numerical investigation conducted by Lan *et al.* [38] found that the predictions by CIDECT [52] are generally unconservative for the strength predictions of high strength steel CHS X-joins made up of steel members with grades of S460, S700, S900 and S1100. Hence, a reduction factor (Q_y) was proposed in the determination of the Q_u. The Q_u proposed by Lan *et al.* [38] was represented by Q_L, as shown in Equations (10) and (11).

$$Q_L = 3.16\left(\frac{1+\beta}{1-0.7\beta}\right)Q_y\gamma^{0.15} \quad (10)$$

$$Q_y = -62\frac{f_{0.2}}{E} + 1.1 \quad (11)$$

The reduction factor of Q_y in Equation (11) accounts for the increased 0.2% proof stress (yield strength) due to the higher steel grades. The Equation (10) was validated for CHS X-joints made up of

steel members with $f_{0.2,n}$ ranging from 700 MPa to 1100 MPa, $0.2 \leq \beta \leq 1.0$ and $2\gamma \leq 30.0$. In this study, the Equations (10)-(11) suggested by Lan *et al.* [38] were also used together with Equation (3) in the nominal strength predictions of the CFHSS CHS X-joints in this study.

5.3 *Comparison of test and numerical strengths with predicted strengths*

The test strengths (P_t) and numerical strengths (P_{FE}) obtained in this study were compared with the nominal strengths predicted by CIDECT [52], EN 1993-1-8 [55], Wardenier [66] and Lan *et al.* [38], as represented by $P_{CDT,n}$, $P_{EC,n}$, P_W and P_L, respectively. It should be noted that the test strengths (P_t) were taken as P_u for specimens of 89×4^-89×4*, 89×4*-89×4* and 89×4^-89×4^ (see Table 4) as the peak loads occurred before the 3%d_0 chord face indentation. Whilst, the rest of the test strengths (P_t) were taken as $P_{EF\text{-}0.03}$ from the verified FEM (discussed in Section 3.2). The detail comparisons of P_t/P_{CDT}, P_t/P_{EC}, P_t/P_W and P_t/P_L are shown in Table 9; and those of $P_{FE}/P_{CDT,n}$, $P_{FE}/P_{EC,n}$, P_{FE}/P_W and P_{FE}/P_L are shown in Tables 10(a)-(c) for specimen Series A, B and C, respectively.

For the comparisons with the test results, it was found that the current predictions are unconservative, however, the equations proposed by Lan *et al*. [38] provided the least unconservative and least scattered predictions. The mean values of $P_t/P_{CDT,n}$, $P_t/P_{EC,n}$, P_t/P_W and P_t/P_L are 0.88, 0.91, 0.67 and 0.93, with the corresponding COVs of 0.147, 0.139, 0.136 and 0.119 (see Table 9). The reduction factors suggested in CIDECT [52] and EN 1993-1-8 [55] improved the predictions in a less unconservative manner when compared with those predicted by Wardernier [66]. Similarly, the predictions by the design rules are also unconservative when compared with the results obtained from the parametric studies except those predicted by Lan *et al.* [38] for specimens Series A (mean value of $P_{FE}/P_L = 1.00$ as shown in Table 10(a). Generally, the predictions tended to be more unconservative as the outer diameter (d_0) of the chords becomes larger except for those predicted by Wardernier [66]. For example, the mean values of $P_{FE}/P_{CDT,n}$ are 0.89, 0.83 and 0.72 for specimens Series A, B and C, respectively, as shown in Tables

10(a)-(c). All these comparisons by using the four design rules are further illustrated in Figures 23-26, respectively. The vertical axis of the figures plots the strength predictions while the horizontal axis plots the test and numerical results. Overall, it was found that the predictions by the current design rules are unconservative.

6. Proposed design rules and predictions

Efforts were made in this section to improve predictions of the CFHSS CHS X-joints. As discussed earlier, the strengths (P) of the X-joints that failed by chord plastification are a function of the $f_{0.2}t_0^2$ (see Equation (3)), and the Q_u (see Equation (4)) that are related to the geometric ratios of β and 2γ, as also illustrated in Figures 20 and 22. Hence, by referring to Equation (6) and Equation (9), both the P_t and P_{FE} in this study were divided by $f_{0.2}t_0^2\gamma^{0.15}$ and $f_{0.2}t_0^2(2\gamma)^{-0.05}$. In addition, the test results of high strength steel CHS X-joints subjected to compression in braces without chord preloading collected from the literature [35,36,58] were also used. Detail information of these test specimens [35,36,58] are shown in Table 11. All the results divided by $f_{0.2}t_0^2\gamma^{0.15}$ and $f_{0.2}t_0^2(2\gamma)^{-0.05}$ are plotted against the corresponding values of β, as shown in Figures 27-28, respectively.

It is shown that the values of $P/f_{0.2}t_0^2\gamma^{0.15}$ and $P/f_{0.2}t_0^2(2\gamma)^{-0.05}$ increased regularly as the values of β increased. However, the values of $P/f_{0.2}t_0^2\gamma^{0.15}$ were relatively more scattered than those of $P/f_{0.2}t_0^2(2\gamma)^{-0.05}$. Hence, the relationship between $P/f_{0.2}t_0^2(2\gamma)^{-0.05}$ and β were derived and plotted as shown in Figure 28. The relationship of Q_u (represented by Q_P) with β and 2γ was proposed as shown in the following Equation (12).

$$Q_P = (22\beta^{2.5} + 4)(2\gamma)^{-0.05} \quad (12)$$

The proposed Equation (12) was used together with Equation (3) to predict the nominal strength (P_P) of the X-joint specimens obtained in this study, as shown in Tables 9-10. The predictions were generally improved when compared with other four predictions, as the unconservative predictions became

conservative or less unconservative. Furthermore, the predictions became less scattered, as reflected by the minimum value of COV in each table.

The test strengths obtained from the literature [35,36,58] were also used to compare with the predictions, as shown in Table 11. Overall, the existing predictions are unconservative except for those predicted by EN-1993-1-8 [55] with the mean value of $P_t/P_{EC,n}$ equal to 1.02. The predictions by using the Equation (3) together with the newly proposed Q_P in Equations (12) provided conservative predictions as reflected in the mean value of P_t/P_P equal to 1.08 with the COV of 0.168. Table 12 further summarized all the comparisons between test and numerical strengths with predictions. Totally, 33 test results and 69 numerical results (the 6 specimens failing in local buckling of the braces but not in chord plastification were not included) were used in the comparisons. Overall, it is shown that all the existing design rules provided unconservative predictions. The EN-1993-1-8 [55] and Lan *et al.* [38] provided the least unconservative predictions with both the mean value of 0.92, However, the EN-1993-1-8 [55] provided less scattered predictions due to the smaller value of COV equal to 0.134. On the contrary, the predictions by using Equation (3) with the proposed Equation (12) provided conservative predictions, i.e., mean value and COV of 1.04 and 0.127, respectively. The test results from the literature [35,36,58] are also plotted in the comparisons as shown in Figures 23-26. The comparisons P_P against P_t and P_{FE} are shown in Figure 29.

7. Conclusions

Experimental and numerical investigations on cold-formed high strength steel (CFHSS) CHS X-joints have been presented. The CFHSS circular members had nominal 0.2% proof stress ($f_{0.2,n}$) up to 1100 MPa. In total, 17 X-joints were tested by applying axial compression through the braces without preloading in chords. The X-joints failed by chord plastification. Non-linear finite element model (FEM) was developed for the CFHSS CHS X-joints. Parametric studies were performed by using the verified

FEM. The key parameters of β, 2γ and τ were designed in the range of 0.2 to 1.0, 10 to 50 and 0.2 to 1.0, respectively. The X-joints had the outer diameter of the chord (d_0) up to 508 mm. The chord plastification failure of the X-joints was mainly found in the numerical study, which was used in the analysis.

The relationship between the joint strengths and the variation of geometric ratios were investigated. It was found that as the β increased, the joint strengths increased in a similar manner regardless of different sets of τ and 2γ. On the contrary, as the 2γ increased, the joint strengths decreased but still in a similar manner for different sets of β and τ. The variation of τ had limited effects on the joint strengths. The CHFSS CHS X-joins showed good deformation capacity and ductility, particularly for those with d_0 of 273 and 508 mm, as all these specimens reached the chord face indentation of $3\%d_0$ even they did not reach the peak loads.

The strengths of the X-joints obtained in this study together with the test strengths collected from the literature [35,36,58] were used to compare with the predictions by using the existing design rules, including those specified in CIDECT [52] and EN-1993-1-8 [55], as well as those proposed by Wardenier [66] and Lan *et al*. [38]. It was found that the current predictions generally provided unconservative predictions, namely overestimated the CFHSS CHS X-joint strengths. The predictions by EN-1993-1-8 [55] and Lan *et al*. [38] provided the least unconservative predictions. A new equation for Q_P that considering the effects of geometric ratios on the strengths was derived based on both the test and numerical results. By adopting the newly proposed equation, the predictions were improved (at the conservative side), and provided the least scattered results when compared with the other predictions. The newly proposed Q_P is applicable to the nominal strength predictions of CFHSS CHS X-joints subjected to axial loading in braces without pre-loading in chords. The X-joints are made up of circular tubes with $f_{0.2,n}$ from 700 MPa to 1100 MPa, $\theta = 90^o$, β, τ and 2γ ranged from 0.17 to 1.00, 0.20 to 2.77 and 10 to 50.

Acknowledgements

The authors are grateful to Rautaruukki for supplying the cold-formed high-strength steel test specimens. Thanks are due to Wo Lee Steel Co. Ltd. (Hong Kong) for using their welding facilities. The research work described in this paper was supported by a grant from the Research Grants Council of the Hong Kong Special Administrative Region, China (Project No. 17210218). The authors wish to acknowledge the support provided by the Chinese National Engineering Research Centre for Steel Construction (Hong Kong Branch) at the Hong Kong Polytechnic University which is funded by the Innovation and Technology Fund administrated by the Innovation and Technology Commission of the Commissioner of the Government of Hong Kong SAR.

References

[1] Ma J.L, Chan T.M., Young B. "Tests on high-strength steel hollow sections: a review" Proceedings of the Institution of Civil Engineers-Structures and Buildings 2017; (9)170, 621-630.

[2] EN-1993-1-12. Eurocode 3: design of steel structures - Part 1-12: Additional rules for the extension of EN 1993 up to steel grades S700., EN 1993-1-12 Brussels, Belgium: CEN, 2007.

[3] AISC/AISI. Specification for structural steel buildings., AISC 360–10, Illinois: American Institute of Steel Construction, Chicago, 2010.

[4] AS 4100. Amendment no.1 to AS 4100–1998 steel structures. AS 4100-A1, Australia: Australian Standard; Sydney, Australia, 2012.

[5] Qiang X., Bijlaard F., Kolstein. H. "Post-fire performance of very high strength steel S960", Journal of Constructional Steel Research 2013; 80, 235-242.

[6] Heidarpour A., Tofts S., Korayem H., Zhao X.L., Hutchinson R. "Mechanical properties of very high strength steel at elevated temperatures", Fire Safety Journal 2014; 64, 27-35.

529 [7] Azhari F., Heidarpour A., Zhao X.L. and Hutchinson R. “Mechanical properties of ultra-high
530 strength (Grade 1200) steel tubes under cooling phase of a fire: An experimental investigation”,
531 Construction and Building Materials 2015; 93, 841-850.
532 [8] Ma J.L., Chan T.M., Young B. “Material properties and residual stresses of cold-formed high
533 strength steel hollow sections”, Journal of Constructional Steel Research 2015; 109, 152-165.
534 [9] Wang J., Afshan S., Schillo N., Theofanous M., Feldmann M., Gardner L. “Material properties
535 and compressive local buckling response of high strength steel square and rectangular hollow sections”,
536 Engineering Structures 2017; 130, 297-315.
537 [10] Fang H., Chan, T.M., Young, B. “Material properties and residual stresses of octagonal high
538 strength steel hollow sections”, Journal of Constructional Steel Research 2018; 148, 479-490.
539 [11] Liu X. Chung K.F. “Experimental and numerical investigation into temperature histories and
540 residual stress distributions of high strength steel S690 welded H-sections”, Engineering Structure
541 2018; 165, 396-411.
542 [12] Jiao H., Zhao X.L. “Section slenderness limits of very high strength circular steel tubes in
543 bending”, Thin-Walled Structures 2004; 42(9),1257-71.
544 [13] Wang J., Afshan S., Gkantou M., Theofanous M., Baniotopoulos C., Gardner L. “Flexural
545 behaviour of hot-finished high strength steel square and rectangular hollow sections”, Journal of
546 Constructional Steel Research 2016; 121, 97-109.
547 [14] Ma J.L., Chan T.M., Young B. “Experimental investigation of cold-formed high strength steel
548 tubular beams”, Engineering Structures 2016; 126, 200-209.
549 [15] Ma J.L., Chan T.M., Young B. “Design of cold-formed high strength steel tubular beams”,
550 Engineering Structures 2017; 151, 432-443.

[16] Javidan F., Heidarpour A., Zhao X.L., Minkkinen J. “Application of high strength and ultra-high strength steel tubes in long hybrid compressive members: Experimental and numerical investigation”, Thin-Walled Structures 2016; 102, 273-285.

[17] Nassirniaa M., Heidarpour A., Zhao X.L., Minkkinen J. “Innovative hollow columns comprising corrugated plates and ultra high-strength steel tubes”, Thin-Walled Structures 2016; 101, 14-25.

[18] Wang J., Gardner L. “Flexural buckling of hot-finished high-strength steel SHS and RHS columns”, Journal of Structural Engineering 2017; 143 (6), 04017028.

[19] Fang, H., Chan, T.M., Young, B. “Structural performance of cold-formed high strength steel tubular columns”, Engineering Structures 2018; 177, 473-488.

[20] Ma J.L., Chan T.M., Young B. “Design of Cold-Formed High-Strength Steel Tubular Stub Columns”, Journal of Structural Engineering 2018; 144(6), 04018063.

[21] Fang, H., Chan, T.M., Young, B. “Behavior of Octagonal High-Strength Steel Tubular Stub Columns”, Journal of Structural Engineering 2019; 145(12), 04019150.

[22] Fang H., Chan T.M. “Buckling resistance of welded high-strength-steel box-section members under combined compression and bending”, Journal of Constructional Steel Research 2019; 162, 105711.

[23] Su A., Liang Y., Zhao O. “Experimental and numerical studies of S960 ultra-high strength steel welded I-section columns”, Thin-Walled Structures 2020; 107166.

[24] Wang F., Liang Y., Zhao O., Young B. “Pin-ended press-braked S960 ultra-high strength steel angle section columns: Testing, numerical modelling and design”, Engineering Structures 2020; 111418.

[25] Fang H., Chan T.M., Young B. “Experimental and Numerical Investigations of Octagonal High-Strength Steel Tubular Stub Columns under Combined Compression and Bending”, Journal of Structural Engineering 2021; 147(1), 04020282.

574 [26] Može P., Beg D., Lopatič J. “Net cross-section design resistance and local ductility of elements
575 made of high strength steel”, Journal of Constructional Steel Research 2007; 63 (11), 1431-1441.
576 [27] Može P., Beg D. “High strength steel tension splices with one or two bolts”, Journal of
577 Constructional Steel Research 2010; 66 (8-9), 1000-1010.
578 [28] Wang Y.B., Lyu Y.F., Li G.Q., Liew R.J.Y. “Behavior of single bolt bearing on high strength
579 steel plate”, Journal of Constructional Steel Research 2017; 137, 19-30.
580 [29] Lyu Y.F., Li G.Q., Wang Y.B., Li H., Wang Y.Z. “Bearing behaviour of multi-bolt high strength
581 steel connections”, Engineering Structure 2020; 212, 110510.
582 [30] Lyu Y.F., Li G.Q., Wang Y.B. “Behavior-Based Resistance Model for Bearing-Type Connection
583 in High-Strength Steels”, Journal of Structure Engineering 2020; 146(7), 04020109.
584 [31] Jiang K., Zhao O., Tan K.H. “Experimental and numerical study of S700 high strength steel
585 double shear bolted connections in tension”; Engineering Structures 2020; 225, 111175.
586 [32] Cho Y.H., Teh L.H., Young B., Ahmed A. “Net section tension strength of bolted connections
587 in ultra-high strength sheet steel exposed to fire.” Journal of Constructional Steel Research 2020; 106237.
588 [33] Cho Y.H., Teh L.H., Ahmed A., Young B. “Material ductility and temperature effects on block
589 shear capacity of bolted connections” Journal of Constructional Steel Research 2020; 106461.
590 [34] Fleischer O., Herion S., Puthli R. “Numerical investigations on the static behaviour of CHS X-
591 joints made of high strength steels”, Tubular Structures XII: Proceedings of Tubular Structures XII,
592 Shanghai, China 2009, pp. 597-605.
593 [35] Puthli R, Bucak O, Herion S, Fleischer O, Fischl A, Josat O. “Adaptation and extension of the
594 valid design formulae for joints made of high-strength steels up to S690 for cold-formed and hot-rolled
595 sections”, CIDECT Report 5BT-7/10 (Draft Final Report) Germany: CIDECT; 2011.

596 [36] Lee C.H., Kim S.H., Chung D.H., Kim D.K., Kim J.W. “Experimental and numerical study of
597 cold-formed high-strength steel CHS X-joints”, Journal of Structure Engineering 2017; 143(8),
598 04017077.
599 [37] Lan X.Y., Chan T.M., Young B. “Static strength of high strength steel CHS X-joints under axial
600 compression”, Journal of Constructional Steel Research 2017; 138, 369-79.
601 [38] Lan X.Y., Chan T.M., Young B. “Structural behaviour and design of chord plastification in high
602 strength steel CHS X-joints”, Construction Building Materials 2018; 191, 1252-67.
603 [39] Lan X.Y., Chan T.M., Young B. “Structural behaviour and design of high strength steel RHS X-
604 joints”, Engineering Structure 2019; 200, 109494.
605 [40] Pandey M., Young B. “Tests of cold-formed high strength steel tubular T-joints”, Thin-Walled
606 Structures 2019; 143, 106200.
607 [41] Pandey M., Young B. “Compression capacities of cold-formed high strength steel tubular T-
608 joints”, Journal of Constructional Steel Research 2019; 162, 105650.
609 [42] Pandey M., Young B. “Structural performance of cold-formed high strength steel tubular X-
610 Joints under brace axial compression”, Engineering Structures 2020; 208, 109768.
611 [43] Su M., Cai Y., Chen X., Young B. “Behaviour of concrete-filled cold-formed high strength steel
612 circular stub columns”, Thin-walled Structures 2020, 157, 107078.
613 [44] Cai Y., Su M., Chen X., Young B. “High strength steel square and rectangular tubular stub
614 columns infilled with concrete”, Journal of Constructional Steel Research 2020; under review.
615 [45] Zhao X.L., Wardenier J., Packer J.A., van der Vegte G. J. “Current static design guidance for
616 hollow-section joints”, Proceedings of the Institution of Civil Engineers Structures and Buildings 2010;
617 163, 361-373.

618 [46] Zhao X.L., Tong L.W. “New Development in Steel Tubular Joints”, Advances in Structural
619 Engineering 2011; 14(4); 699-715.
620 [47] IIW (1981). Design Recommendations for Hollow Section Joints – Predominantly Statically
621 Loaded, 1st Edition, IIW Doc. XV-491- 81, IIW Annual Assembly, Lisbon, Portugal.
622 [48] IIW (1989). Design Recommendations for Hollow Section Joints – Predominantly Statically
623 Loaded, 2nd Edition, IIW Doc. XV- 701-89, IIW Annual Assembly, Helsinki, Finland.
624 [49] IIW (2009). IIW Static Design Procedure for Welded Hollow Section Joints – Recommendations,
625 IIW Doc. XV-1329–09, IIW Annual Assembly, Singapore.
626 [50] Wardenier J., Kurobane Y., Packer J.A., Dutta D., Yeomans, N. “Design Guide for Circular
627 Hollow Section (CHS) Joints under Predominantly Static Loading”, TÜV-Verlag, Köln, Germany, 1991.
628 [51] Packer J.A., Wardenier J., Kurobane Y., Dutta D., Yeomans, N. “Design Guide for Rectangular
629 Hollow Section (RHS) Joints under Predominantly Static Loading”, TÜV-Verlag, Köln, Germany, 1992.
630 [52] Wardenier J., Kurobane Y., Packer J.A., van der Vegte G.J., Zhao X.L. “Design Guide for
631 Circular Hollow Section (CHS) Joints under Predominantly Static Loading”, CIDECT Design Guide No.
632 1, 2nd Edition, CIDECT, Geneva, Switzerland, 2008.
633 [53] Packer J.A., Wardenier J., Zhao X.L., van der Vegte G.J., Kurobane, Y. “Design Guide for
634 Rectangular Hollow Section (RHS) Joints under Predominantly Static Loading”, CIDECT Design Guide
635 No. 3, 2nd Edition, CIDECT, Geneva, Switzerland, 2009.
636 [54] Packer J.A., Henderson J.E. “Hollow Structural Section Connections and Trusses - A Design
637 Guide”, Canadian Institute of Steel Construction (CISC), Willowdale, Ontario, Canada, 1997.
638 [55] EN 1993-1-8. Eurocode 3: Design of Steel Structures - Part 1.8: Design of Joints, European
639 Committee for Standardization (CEN), Brussels, Belgium, 2005.

[56] BS ISO 14346, Static design procedure for welded hollow-section joints – Recommendations, British Standard International Standards, Geneva, Switzerland, 2013.

[57] Togo, T. “Experimental study on mechanical behaviour of tubular joints”, Ph.D. Thesis, Osaka University, Japan, (in Japanese), 1967.

[58] Lan X.Y., Chan T.M., Young B. “Experimental study on the behaviour and strength of high strength steel CHS T- and X-joints”, Engineering Structures 2020; 206, 110182

[59] NAS. “North American Specification for the design of cold-formed steel structural members.” North American Specification (NAS), AISI S100–16, Washington D. C., USA: American Iron and Steel Institute (AISI), 2016.

[60] Cai Y., Chan T.M., Young B. “Experimental investigation on cold-formed high strength steel tubular T-joints”, The 9th International Conference on Advances in Steel Structures (ICASS2018), 2018, Hong Kong, China, Paper No. 009, Full paper in drive.

[61] AWS D1.1M. Structural Welding Code-Steel, American Welding Society, AWS D1.1/1.1M, Miami, FL, USA, 2015.

[62] AWS A5.28M. Specification for Low-Alloy Steel Electrodes and Rods for Gas Shielded Arc Welding, American Welding Society, AWS A5.28/A5.28M: 2005, Miami, FL, USA, 2015.

[63] ABAQUS. (2019). “Analysis User’s Manual”, ABAQUS, Inc., Version 6.20, 2019.

[64] Lu L.H., de Winkel G.D., Yu Y., Wardenier J. “Deformation limit for the ultimate strength of hollow section joints”, Tubular structures VI. Melbourne: Balkema; 1994. p. 341-347.

[65] van der Vegte G.J., Wardenier J, Zhao X.L., Packer J.A. “Evaluation of new CHS strength formulae to design strengths”, Tubular Structures XII. London: CRC Press; 2009; 313-22.

[66] Wardenier J. Hollow section joints. The Netherlands: Delft University Press; 1982.

Table 1: Measured dimensions of CFHSS circular tubular X-joints

Specimens	Upper braces (mm)			Lower braces (mm)			Chords (mm)			Geometric ratios		
Brace - Chord	d_1	t_1	l_1	d_1	t_1	l_1	d_0	t_0	l_0	β	τ	2γ
22×4 - 133×4	22.0	3.96	46.9	22.0	3.79	46.4	133.0	3.93	601.5	0.17	0.96	33.84
55×11 - 133×4	55.3	10.4	112.4	55.3	10.6	112.4	134.1	3.95	635.4	0.41	2.63	33.95
89×4^ - 133×4	89.3	3.94	179.8	88.6	3.91	179.2	134.5	3.93	668.3	0.66	0.99	34.22
89×4* - 133×4	89.3	3.93	179.4	89.2	3.92	179.3	134.3	3.97	669.7	0.66	0.99	33.83
22×4 - 108×4	22.0	3.79	46.2	22.0	3.83	46.2	107.7	3.91	526.5	0.20	0.97	27.54
55×11 - 108×4	55.4	10.6	112.1	55.2	10.7	112.4	107.9	3.93	559.8	0.51	2.70	27.46
89×4^ - 108×4	88.8	3.91	179.4	89.2	3.91	179.2	108.1	3.92	594.5	0.82	1.00	27.58
89×4* - 108×4	89.1	3.94	179.8	88.5	3.87	179.2	108.1	3.82	593.6	0.82	1.01	28.30
22×4 - 89×4*	22.1	3.89	45.7	22.1	3.95	46.4	88.8	3.92	470.4	0.25	0.99	22.65
55×11 - 89×4*	55.1	10.8	111.5	55.2	10.6	112.2	88.8	3.83	505.5	0.62	2.77	23.19
55×11 - 89×4*-r	55.1	10.6	111.9	55.2	10.6	111.8	89.0	3.91	503.4	0.62	2.71	22.76
89×4^ - 89×4*	89.1	3.89	180.2	88.6	3.92	179.7	88.7	3.89	537.8	1.00	1.00	22.80
89×4* - 89×4*	89.0	3.93	180.5	89.1	3.86	180.2	89.3	3.93	538.1	1.00	0.98	22.72
22×4 - 89×4^	22.1	3.81	46.1	22.1	3.89	46.3	88.9	3.91	470.2	0.25	0.97	22.74
22×4 - 89×4^-r	22.1	3.82	46.3	22.1	3.89	46.2	88.9	3.89	470.5	0.25	0.98	22.85
55×11 - 89×4^	55.2	10.6	112.2	55.1	10.8	112.4	89.1	3.96	503.5	0.62	2.68	22.50
89×4^ - 89×4^	88.6	3.90	180.3	89.1	3.90	179.8	89.0	3.93	535.9	1.00	0.99	22.65

Note: ^ and * mean having nominal 0.2% proof stress of 900 MPa and 1100 MPa, respectively.

Table 2: Measured welding details of CFHSS circular tubular X-joint specimens

Specimens	Δ_1 (mm)	Δ_2 (mm)	Δ_3 (mm)	Δ_4 (mm)	w (mm)
22×4 - 133×4	5.78	5.63	4.25	-	-
55×11 - 133×4	6.20	5.08	4.48	-	-
89×4^ - 133×4	5.68	5.53	4.54	-	-
89×4* - 133×4	5.43	5.30	4.12	-	-
22×4 - 108×4	5.93	5.28	4.77	-	-
55×11 - 108×4	5.70	4.95	3.65	-	-
89×4^ - 108×4	5.50	6.03	4.72	-	-
89×4* - 108×4	5.55	5.58	4.60	-	-
22×4 - 89×4*	6.15	5.93	4.60	-	-
55×11 - 89×4*	6.38	5.58	4.97	-	-
55×11 - 89×4*-r	6.35	4.80	4.45		
89×4^ - 89×4*	5.50	6.15	4.89	19.74	1.75
89×4* - 89×4*	5.70	6.18	4.61	19.41	1.49
22×4 - 89×4^	5.70	5.80	4.46	-	-
22×4 - 89×4^-r	5.85	5.48	4.43	-	-
55×11 - 89×4^	6.40	5.33	4.98	-	-
89×4^ - 89×4^	5.35	6.43	4.61	20.77	1.35

Note: ^ and * mean having nominal 0.2% proof stress of 900 MPa and 1100 MPa, respectively.

Table 3: Measured material properties of CFHSS circular tubes

Sections	Measured								
$D\times t$	E	$f_{0.01}$	$f_{0.2}$	f_u	ε_u	ε_f	n	$f_{0.2}/f_u$	$0.8f_u$
mm	GPa	MPa	MPa	MPa	%	%			MPa
22×4	197	501.0	755	832	1.6	5.4	7.3	0.91	665.6
55×11	204	606.0	800	919	4.4	8.6	10.8	0.87	735.2
89×4^	212	515.0	983	1106	2.1	11.7	4.6	0.89	884.8
89×4*	207	585	1213	1313	2.4	10.6	4.1	0.92	1050.4
108×4	203	553	1155	1344	2.3	10.9	4.1	0.86	1075.2
133×4	207	535	1100	1255	2.7	10.7	4.2	0.88	1004.0

Note: ^ and * mean having nominal 0.2% proof stress of 900 MPa and 1100 MPa, respectively.

Table 4: Test results and FE predictions of CFHSS circular tubular X-joints

Specimens	Axial shortening (mm)		Tests (kN)		FEA (kN)		Comparison	
	$\mu_{0.03}$	μ_u	$P_{3\%}$	P_u	$P_{FE\text{-}1}$	$P_{FE\text{-}u}$	$P_{3\%}/P_{FE\text{-}1}$	$P_u/P_{FE\text{-}u}$
22×4 - 139×6	3.99	8.30	63.5	82.5	60.9	79.8	1.04	1.03
55×11 - 139×6	4.02	9.38	88.8	123.0	100.8	133.7	0.88	0.92
89×4^ - 139×6	4.04	7.61	157.8	179.0	162.5	196.0	0.97	0.91
89×4* - 139×6	4.03	7.61	161.1	182.4	164.6	198.0	0.98	0.92
22×4 - 108×4	3.23	6.45	76.7	100.1	71.3	94.5	1.08	1.06
55×11 - 108×4	3.24	7.23	120.5	147.9	130.9	166.4	0.92	0.89
89×4^ - 108×4	3.24	5.46	224.6	232.4	250.5	264.2	0.90	0.88
89×4* - 108×4	3.24	4.35	221.9	227.7	239.3	253.5	0.93	0.90
22×4 - 89×4*	2.66	6.34	86.4	112.1	83.7	108.3	1.03	1.04
55×11 - 89×4*	2.66	5.66	163.5	183.3	166.1	191.6	0.98	0.96
55×11 - 89×4*-r	2.67	5.45	152.9	173.8	-	-	-	-
89×4^ - 89×4*	2.66	1.83	431.2	441.3	447.3	480.8	0.96	0.92
89×4* - 89×4*	2.68	1.94	442.2	454.1	449.9	492.1	0.98	0.92
22×4 - 89×4^	2.67	5.81	83.8	102.9	78.4	95.2	1.07	1.08
22×4 - 89×4^-r	2.67	5.49	74.7	92.4	-	-	-	-
55×11 - 89×4^	2.67	4.91	146.6	161.0	159.4	177.6	0.92	0.91
89×4^ - 89×4^	2.67	1.84	412.3	421.9	407.1	444.0	1.01	0.95
						Mean	0.98	0.95
						COV	0.062	0.070

Note: ^ and * mean having nominal 0.2% proof stress of 900 MPa and 1100 MPa, respectively.

Table 5: Specimens of CFHSS circular tubular X-joints in parametric studies

Series	Braces (mm)		Chords (mm)		Geometric ratios		
	d_1	t_1	d	t	β	τ	2γ
Series A	[17.78~88.90]	6.30	88.9	6.30	0.20, 0.30, 0.40, 0.50, 0.60, 0.70, 0.80, 0.90, 1.00	1.00	14.11
	35.56	[1.26~6.30]		6.30	0.40	0.20, 0.30, 0.40, 0.50, 0.60, 0.70, 0.80, 0.90, 1.00	14.11
	35.56	[1.78~8.89]		1.78, 1.98, 2.22, 2.54, 2.96, 3.56, 4.45, 6.30, 8.89	0.40	1.00	10.00, 14.11, 19.98, 24.97, 30.03, 35.00, 40.05, 44.90, 49.94
Series B	[54.60~273.00]	7.50	273.0	12.50	0.20, 0.30, 0.40, 0.50, 0.60, 0.70, 0.80, 0.90, 1.00	0.60	21.84
	163.80	[2.50~12.50]		12.50	0.60	0.20, 0.30, 0.40, 0.50, 0.60, 0.70, 0.80, 0.90, 1.00	21.84
	163.80	[3.28~16.38]		5.46, 6.07, 6.83, 7.80, 9.10, 10.92, 12.50, 18.20, 27.30	0.60	0.60	10.00, 15.00, 21.84, 25.00, 30.00, 35.00, 39.97, 44.98, 50.00
Series C	[101.60~508.00]	5.00	508.0	12.50	0.20, 0.30, 0.40, 0.50, 0.60, 0.70, 0.80, 0.90, 1.00	0.40	40.64
	406.40	[2.50~12.50]		12.50	0.80	0.20, 0.30, 0.40, 0.50, 0.60, 0.70, 0.80, 0.90, 1.00	40.64
	406.40	[4.06~20.32]		10.16, 11.29, 12.50, 14.51, 16.93, 20.32, 25.40, 33.87, 50.80	0.80	0.40	10.00, 15.00, 20.00, 25.00, 30.01, 35.01, 40.64, 45.00, 50.00

Table 6: Parametric study results and strength comparisons for X-joints Series A (d_0 = 88.9 mm)

Specimens	Geometric ratios			P_{FE}	Normalized
Brace - Chord	β	τ	2γ	(kN)	
17.78×6.30 - 88.90×6.30	0.20	1.00	14.11	211.3	0.26
26.67×6.30 - 88.90×6.30	0.30	1.00	14.11	255.2	0.31
35.56×6.30 - 88.90×6.30	0.40	1.00	14.11	306.7	0.38
44.45×6.30 - 88.90×6.30	0.50	1.00	14.11	367.4	0.45
53.34×6.30 - 88.90×6.30	0.60	1.00	14.11	440.4	0.54
62.23×6.30 - 88.90×6.30	0.70	1.00	14.11	532.4	0.65
71.12×6.30 - 88.90×6.30	0.80	1.00	14.11	653.6	0.80
80.01×6.30 - 88.90×6.30	0.90	1.00	14.11	817.2	1.00
88.90×6.30 - 88.90×6.30	1.00	1.00	14.11	1173.5	1.44
35.56×1.26 - 88.90×6.30#	0.40	0.20	14.11	-	-
35.56×1.89 - 88.90×6.30#	0.40	0.30	14.11	-	-
35.56×2.52 - 88.90×6.30	0.40	0.40	14.11	291.7	0.95
35.56×3.15 - 88.90×6.30	0.40	0.50	14.11	297.8	0.97
35.56×3.78 - 88.90×6.30	0.40	0.60	14.11	300.9	0.98
35.56×4.41 - 88.90×6.30	0.40	0.70	14.11	302.9	0.99
35.56×5.04 - 88.90×6.30	0.40	0.80	14.11	304.5	0.99
35.56×5.67 - 88.90×6.30	0.40	0.90	14.11	305.7	1.00
35.56×6.30 - 88.90×6.30	0.40	1.00	14.11	306.7	1.00
35.56×1.78 - 88.90×1.78	0.40	1.00	49.94	17.2	0.12
35.56×1.98 - 88.90×1.98	0.40	1.00	44.90	22.3	0.15
35.56×2.22 - 88.90×2.22	0.40	1.00	40.05	29.3	0.20
35.56×2.54 - 88.90×2.54	0.40	1.00	35.00	40.4	0.28
35.56×2.96 - 88.90×2.96	0.40	1.00	30.03	57.8	0.40
35.56×3.56 - 88.90×3.56	0.40	1.00	24.97	88.4	0.61
35.56×4.45 - 88.90×4.45	0.40	1.00	19.98	145.5	1.00
35.56×6.30 - 88.90×6.30	0.40	1.00	14.11	306.7	2.11
35.56×8.89 - 88.90×8.89	0.40	1.00	10.00	625.1	4.30

Note: # means brace failed by local buckling.

Table 7: Parametric study results and strength comparisons for X-joints Series B (d_0 = 273 mm)

Specimens	Geometric ratios			P_{FE}	Normalized
Brace - Chord	β	τ	2γ	(kN)	
54.60×7.50 - 273.00×12.50	0.20	0.60	21.84	736.0	0.23
81.90×7.50 - 273.00×12.50	0.30	0.60	21.84	902.1	0.28
109.20×7.50 - 273.00×12.50	0.40	0.60	21.84	1090.2	0.34
136.50×7.50 - 273.00×12.50	0.50	0.60	21.84	1319.3	0.41
163.80×7.50 - 273.00×12.50	0.60	0.60	21.84	1606.2	0.50
191.10×7.50 - 273.00×12.50	0.70	0.60	21.84	1973.3	0.62
218.40×7.50 - 273.00×12.50	0.80	0.60	21.84	2472.4	0.77
245.70×7.50 - 273.00×12.50	0.90	0.60	21.84	3201.3	1.00
273.00×7.50 - 273.00×12.50	1.00	0.60	21.84	4920.1	1.54
163.80×2.50 - 273.00×12.50#	0.60	0.20	21.84	-	-
163.80×3.75 - 273.00×12.50	0.60	0.30	21.84	1528.5	0.93
163.80×5.00 - 273.00×12.50	0.60	0.40	21.84	1571.8	0.96
163.80×6.25 - 273.00×12.50	0.60	0.50	21.84	1591.6	0.97
163.80×7.50 - 273.00×12.50	0.60	0.60	21.84	1606.2	0.98
163.80×8.75 - 273.00×12.50	0.60	0.70	21.84	1618.0	0.98
163.80×10.00 - 273.00×12.50	0.60	0.80	21.84	1628.7	0.99
163.80×11.25 - 273.00×12.50	0.60	0.90	21.84	1637.6	1.00
163.80×12.50 - 273.00×12.50	0.60	1.00	21.84	1645.0	1.00
163.80×3.28 - 273.00×5.46	0.60	0.60	50.00	242.6	0.15
163.80×3.64 - 273.00×6.07	0.60	0.60	44.98	311.6	0.19
163.80×4.10 - 273.00×6.83	0.60	0.60	39.97	410.5	0.26
163.80×4.68 - 273.00×7.80	0.60	0.60	35.00	557.6	0.35
163.80×5.46 - 273.00×9.10	0.60	0.60	30.00	792.2	0.49
163.80×6.55 - 273.00×10.92	0.60	0.60	25.00	1193.5	0.74
163.80×7.50 - 273.00×12.50	0.60	0.60	21.84	1606.2	1.00
163.80×10.92 - 273.00×18.20	0.60	0.60	15.00	3548.7	2.21
163.80×16.38 - 273.00×27.30	0.60	0.60	10.00	7969.2	4.96

Note: # means brace failed by local buckling.

Table 8: Parametric study results and strength comparisons for X-joints Series C (d_0 = 508 mm)

Specimens	Geometric ratios			P_{FE}	Normalized
Brace - Chord	β	τ	2γ	(kN)	
101.60×5.00 - 508.00×12.50	0.20	0.40	40.64	589.6	0.20
152.40×5.00 - 508.00×12.50	0.30	0.40	40.64	718.1	0.24
203.20×5.00 - 508.00×12.50	0.40	0.40	40.64	876.5	0.29
254.00×5.00 - 508.00×12.50	0.50	0.40	40.64	1075.8	0.36
304.80×5.00 - 508.00×12.50	0.60	0.40	40.64	1338.8	0.45
355.60×5.00 - 508.00×12.50	0.70	0.40	40.64	1698.1	0.57
406.40×5.00 - 508.00×12.50	0.80	0.40	40.64	2210.1	0.74
457.20×5.00 - 508.00×12.50	0.90	0.40	40.64	2978.2	1.00
508.00×5.00 - 508.00×12.50#	1.00	0.40	40.64	-	-
406.40×2.50 - 508.00×12.50#	0.80	0.20	40.64	-	0.00
406.40×3.75 - 508.00×12.50	0.80	0.30	40.64	2186.1	0.95
406.40×5.00 - 508.00×12.50	0.80	0.40	40.64	2210.1	0.96
406.40×6.25 - 508.00×12.50	0.80	0.50	40.64	2229.3	0.97
406.40×7.50 - 508.00×12.50	0.80	0.60	40.64	2247.0	0.98
406.40×8.75 - 508.00×12.50	0.80	0.70	40.64	2263.4	0.98
406.40×10.00 - 508.00×12.50	0.80	0.80	40.64	2278.1	0.99
406.40×11.25 - 508.00×12.50	0.80	0.90	40.64	2290.6	1.00
406.40×12.50 - 508.00×12.50	0.80	1.00	40.64	2300.8	1.00
406.40×4.06 - 508.00×10.16	0.80	0.40	50.00	1386.3	0.14
406.40×4.52 - 508.00×11.29	0.80	0.40	45.00	1760.0	0.18
406.40×5.00 - 508.00×12.50	0.80	0.40	40.64	2210.1	0.22
406.40×5.81 - 508.00×14.51	0.80	0.40	35.01	3071.4	0.31
406.40×6.77 - 508.00×16.93	0.80	0.40	30.01	4293.5	0.43
406.40×8.13 - 508.00×20.32	0.80	0.40	25.00	6340.5	0.63
406.40×10.16 - 508.00×25.40	0.80	0.40	20.00	10053.0	1.00
406.40×13.55 - 508.00×33.87	0.80	0.40	15.00	17421.9	1.73
406.40×20.32 - 508.00×50.80#	0.80	0.40	10.00	-	-

Note: # means brace failed by local buckling.

Table 9: Strength comparisons between test results obtained from this study and predictions

Specimens	$P_t/P_{CDT,n}$	$P_t/P_{EC,n}$	P_t/P_W	P_t/P_L	P_t/P_P
22×4 - 133×4	0.70	0.59	0.49	0.76	1.03
55×11 - 133×4	0.75	0.74	0.62	0.81	1.11
89×4^ - 133×4	0.79	0.84	0.70	0.83	0.98
89×4* - 133×4	0.78	0.83	0.69	0.83	0.96
22×4 - 108×4	0.74	0.64	0.52	0.84	1.09
55×11 - 108×4	0.79	0.80	0.66	0.89	1.07
89×4^ - 108×4	0.84	0.88	0.73	0.93	0.96
89×4* - 108×4	0.85	0.90	0.74	0.94	0.97
22×4 - 89×4*	0.86	0.69	0.57	0.93	1.15
55×11 - 89×4*	0.92	0.87	0.72	0.98	1.02
89×4^ - 89×4*	1.02	0.85	0.70	1.07	1.08
89×4* - 89×4*	1.03	0.86	0.71	1.09	1.10
22×4 - 89×4^	0.96	0.80	0.66	0.98	1.34
55×11 - 89×4^	0.99	0.97	0.80	1.00	1.15
89×4^ - 89×4^	1.15	1.00	0.82	1.14	1.26
Mean	0.88	0.91	0.67	0.93	1.08
COV	0.147	0.139	0.136	0.119	0.101

Note: ^ and * mean having nominal 0.2% proof stress of 900 MPa and 1100 MPa, respectively.

Table 10: Strength comparisons between parametric study results and predictions

(a) Series A with d_0 = 88.9 mm

Specimens	$P_{FE}/P_{CDT,n}$	$P_{FE}/P_{EC,n}$	P_{FE}/P_W	P_{FE}/P_L	P_{FE}/P_P
17.78×6.30 - 88.90×6.30	0.93	0.72	0.58	1.04	1.20
26.67×6.30 - 88.90×6.30	0.95	0.79	0.63	1.07	1.25
35.56×6.30 - 88.90×6.30[$]	0.97	0.85	0.67	1.09	1.23
44.45×6.30 - 88.90×6.30	0.98	0.89	0.71	1.10	1.16
53.34×6.30 - 88.90×6.30	0.98	0.92	0.73	1.10	1.08
62.23×6.30 - 88.90×6.30	0.98	0.94	0.75	1.10	1.02
71.12×6.30 - 88.90×6.30	0.98	0.94	0.74	1.10	0.98
80.01×6.30 - 88.90×6.30	0.98	0.90	0.72	1.10	0.97
88.90×6.30 - 88.90×6.30	1.08	0.90	0.72	1.21	1.12
35.56×1.26 - 88.90×6.30#	-	-	-	-	-
35.56×1.89 - 88.90×6.30#	-	-	-	-	-
35.56×2.52 - 88.90×6.30	0.92	0.81	0.64	1.03	1.17
35.56×3.15 - 88.90×6.30	0.94	0.82	0.65	1.06	1.19
35.56×3.78 - 88.90×6.30	0.95	0.83	0.66	1.07	1.20
35.56×4.41 - 88.90×6.30	0.96	0.84	0.66	1.07	1.21
35.56×5.04 - 88.90×6.30	0.96	0.84	0.67	1.08	1.22
35.56×5.67 - 88.90×6.30	0.97	0.84	0.67	1.08	1.22
35.56×6.30 - 88.90×6.30[$]	0.97	0.85	0.67	1.09	1.23
35.56×1.78 - 88.90×1.78	0.56	0.59	0.50	0.63	0.92
35.56×1.98 - 88.90×1.98	0.60	0.62	0.53	0.67	0.96
35.56×2.22 - 88.90×2.22	0.64	0.65	0.55	0.72	0.99
35.56×2.54 - 88.90×2.54	0.69	0.69	0.57	0.77	1.04
35.56×2.96 - 88.90×2.96	0.74	0.72	0.60	0.83	1.09
35.56×3.56 - 88.90×3.56	0.80	0.76	0.63	0.90	1.14
35.56×4.45 - 88.90×4.45	0.87	0.80	0.65	0.98	1.19
35.56×6.30 - 88.90×6.30[$]	0.97	0.85	0.67	1.09	1.23
35.56×8.89 - 88.90×8.89	1.04	0.87	0.68	1.17	1.23
Mean	0.89	0.90	0.65	1.00	1.12
COV	0.163	0.123	0.106	0.163	0.093

Note: # means brace failed by local buckling; [$] means identical specimens.

(b) Series B with d_0 = 273 mm

Specimens	$P_{FE}/P_{CDT,n}$	$P_{FE}/P_{EC,n}$	P_{FE}/P_W	P_{FE}/P_L	P_{FE}/P_P
54.60×7.50 - 273.00×12.50	0.77	0.64	0.52	0.86	1.08
81.90×7.50 - 273.00×12.50	0.80	0.71	0.58	0.90	1.15
109.20×7.50 - 273.00×12.50	0.82	0.76	0.62	0.92	1.13
136.50×7.50 - 273.00×12.50	0.84	0.81	0.66	0.94	1.08
163.80×7.50 - 273.00×12.50[$]	0.85	0.86	0.70	0.95	1.02
191.10×7.50 - 273.00×12.50	0.87	0.88	0.72	0.97	0.98
218.40×7.50 - 273.00×12.50	0.88	0.90	0.73	0.99	0.96
245.70×7.50 - 273.00×12.50	0.91	0.89	0.73	1.02	0.99
273.00×7.50 - 273.00×12.50	1.08	0.96	0.78	1.21	1.22
163.80×2.50 - 273.00×12.50#	-	-	-	-	-
163.80×3.75 - 273.00×12.50	0.81	0.81	0.66	0.91	0.98
163.80×5.00 - 273.00×12.50	0.83	0.84	0.68	0.93	1.00
163.80×6.25 - 273.00×12.50	0.84	0.85	0.69	0.95	1.02
163.80×7.50 - 273.00×12.50[$]	0.85	0.86	0.70	0.95	1.02
163.80×8.75 - 273.00×12.50	0.86	0.86	0.70	0.96	1.03
163.80×10.00 - 273.00×12.50	0.86	0.87	0.71	0.97	1.04
163.80×11.25 - 273.00×12.50	0.87	0.87	0.71	0.97	1.04
163.80×12.50 - 273.00×12.50	0.87	0.88	0.71	0.98	1.05
163.80×3.28 - 273.00×5.46	0.60	0.68	0.57	0.67	0.85
163.80×3.64 - 273.00×6.07	0.63	0.70	0.59	0.70	0.87
163.80×4.10 - 273.00×6.83	0.67	0.73	0.61	0.75	0.90
163.80×4.68 - 273.00×7.80	0.71	0.76	0.63	0.79	0.94
163.80×5.46 - 273.00×9.10	0.76	0.80	0.66	0.85	0.97
163.80×6.55 - 273.00×10.92	0.81	0.83	0.68	0.91	1.00
163.80×7.50 - 273.00×12.50[$]	0.85	0.86	0.70	0.95	1.02
163.80×10.92 - 273.00×18.20	0.94	0.89	0.71	1.05	1.05
163.80×16.38 - 273.00×27.30	1.00	0.89	0.70	1.12	1.02
Mean	0.83	0.91	0.67	0.93	1.02
COV	0.130	0.099	0.090	0.130	0.083

Note: # means brace failed by local buckling; [$] means identical specimens.

(c) Series C with d_0 = 508 mm

Specimens	$P_{FE}/P_{CDT,n}$	$P_{FE}/P_{EC,n}$	P_{FE}/P_W	P_{FE}/P_L	P_{FE}/P_P
101.60×5.00 - 508.00×12.50	0.56	0.51	0.43	0.63	0.89
152.40×5.00 - 508.00×12.50	0.58	0.56	0.47	0.65	0.94
203.20×5.00 - 508.00×12.50	0.60	0.61	0.52	0.67	0.94
254.00×5.00 - 508.00×12.50	0.62	0.66	0.56	0.70	0.91
304.80×5.00 - 508.00×12.50	0.65	0.71	0.60	0.72	0.88
355.60×5.00 - 508.00×12.50	0.68	0.76	0.64	0.76	0.87
406.40×5.00 - 508.00×12.50[$]	0.72	0.80	0.67	0.81	0.89
457.20×5.00 - 508.00×12.50	0.77	0.83	0.70	0.87	0.95
508.00×5.00 - 508.00×12.50#	-	-	-	-	-
406.40×2.50 - 508.00×12.50#	-	-	-	-	-
406.40×3.75 - 508.00×12.50	0.71	0.80	0.67	0.80	0.88
406.40×5.00 - 508.00×12.50[$]	0.72	0.80	0.67	0.81	0.89
406.40×6.25 - 508.00×12.50	0.73	0.81	0.68	0.81	0.90
406.40×7.50 - 508.00×12.50	0.73	0.82	0.69	0.82	0.90
406.40×8.75 - 508.00×12.50	0.74	0.82	0.69	0.83	0.91
406.40×10.00 - 508.00×12.50	0.74	0.83	0.70	0.83	0.92
406.40×11.25 - 508.00×12.50	0.75	0.83	0.70	0.84	0.92
406.40×12.50 - 508.00×12.50	0.75	0.84	0.70	0.84	0.92
406.40×4.06 - 508.00×10.16	0.66	0.76	0.65	0.74	0.85
406.40×4.52 - 508.00×11.29	0.69	0.79	0.66	0.78	0.87
406.40×5.00 - 508.00×12.50[$]	0.72	0.80	0.67	0.81	0.89
406.40×5.81 - 508.00×14.51	0.76	0.83	0.69	0.85	0.91
406.40×6.77 - 508.00×16.93	0.80	0.85	0.70	0.89	0.93
406.40×8.13 - 508.00×20.32	0.84	0.87	0.71	0.94	0.94
406.40×10.16 - 508.00×25.40	0.88	0.89	0.72	0.99	0.94
406.40×13.55 - 508.00×33.87	0.90	0.86	0.69	1.01	0.91
406.40×20.32 - 508.00×50.80#	-	-	-	-	-
Mean	0.72	0.86	0.65	0.81	0.91
COV	0.123	0.130	0.125	0.123	0.030

Note: # means brace failed by local buckling; [$] means identical specimens.

Table 11: Strength comparisons between test results of X-joints in literature and predictions

Specimens	$f_{0.2}$ (MPa)	f_u (MPa)	$P_t/P_{CDT,n}$	$P_t/P_{EC,n}$	P_t/P_W	P_t/P_L	P_t/P_P
R32[a]	730	800	1.23	1.15	0.95	1.11	1.45
R33[a]	739	798	1.10	0.97	0.79	0.98	1.21
R42[a]	727	793	1.18	0.98	0.81	1.06	1.25
R68[a]	904	946	1.06	0.93	0.76	0.97	1.08
R69[a]	858	879	1.18	0.93	0.76	1.04	1.38
R70[a]	847	892	1.08	0.95	0.77	0.97	1.00
R71[a]	854	900	1.08	0.98	0.80	0.97	1.07
R72[a]	894	937	1.03	0.89	0.73	0.94	1.14
R74[a]	811	863	1.11	0.93	0.75	1.00	1.04
R75[a]	811	863	1.05	0.89	0.71	0.94	0.92
X90-650-0.75-16[b]	764	905	1.08	1.07	0.85	1.06	1.14
X90-650-0.62-26[b]	798	914	1.03	1.05	0.86	0.99	1.24
X1[c]	972	1107	0.80	0.87	0.74	0.82	1.03
X2[c]	972	1107	0.76	0.85	0.73	0.78	0.96
X3[c]	972	1107	0.50	0.57	0.49	0.51	0.66
X4[c]	972	1107	0.74	0.83	0.71	0.76	1.04
X5[c]	1012	1119	0.81	0.86	0.73	0.82	0.96
X6[c]	990	1114	0.77	0.85	0.72	0.77	0.95
Total 18 tests	Mean		0.98	1.02	0.76	0.92	1.08
	COV		0.202	0.132	0.121	0.159	0.168

Note: [a], [b] and [c] mean presented in Refs. [35], [36] and [58], respectively.

Table 12: Overall comparisons of test and numerical results with predictions

Specimens	Number		$P_t/P_{CDT,n}$ ($P_{FE}/P_{CDT,n}$)	$P_t/P_{EC,n}$ ($P_{FE}/P_{EC,n}$)	P_t/P_W (P_{FE}/P_W)	P_t/P_L (P_{FE}/P_L)	P_t/P_P (P_{FE}/P_P)
Tests	33	Mean	0.93	0.97	0.72	0.92	1.08
		COV	0.187	0.145	0.138	0.140	0.139
Parametric studies	69	Mean	0.81	0.89	0.65	0.91	1.02
		COV	0.165	0.118	0.107	0.165	0.115
Total	102	Mean	0.85	0.92	0.68	0.92	1.04
		COV	0.185	0.134	0.127	0.156	0.127

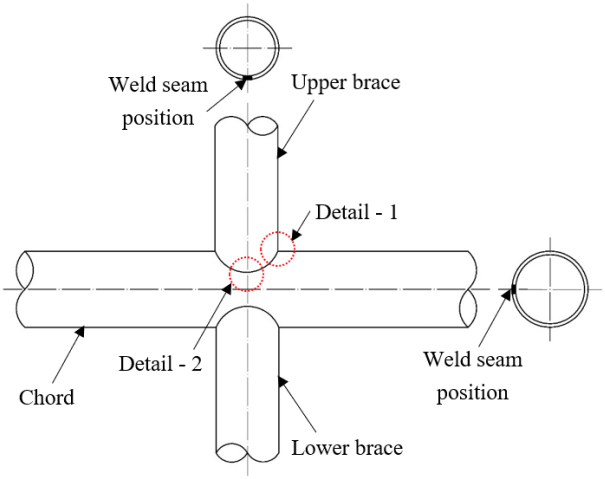

Fig. 1: Schematic view of CFHSS CHS X-joint

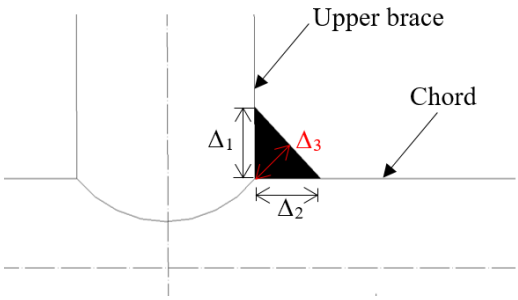

(a) Welding "Detail 1"

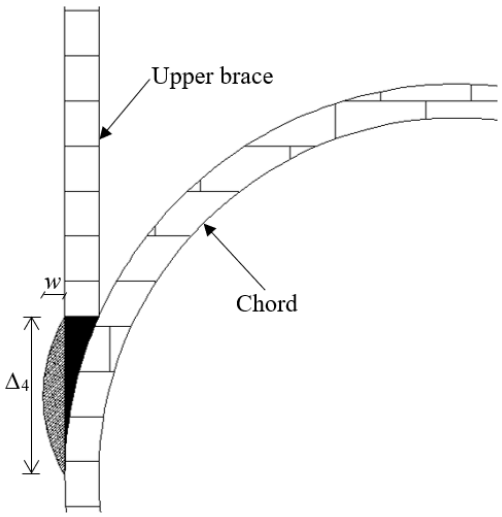

(b) Side view of welding "Detail 2" for specimens with β = 1.00

Fig. 2: Welding details of CFHSS CHS X-joint

Fig. 3: Measurement of welding details Δ_3 at toe for specimen 89×4* - 89×4*

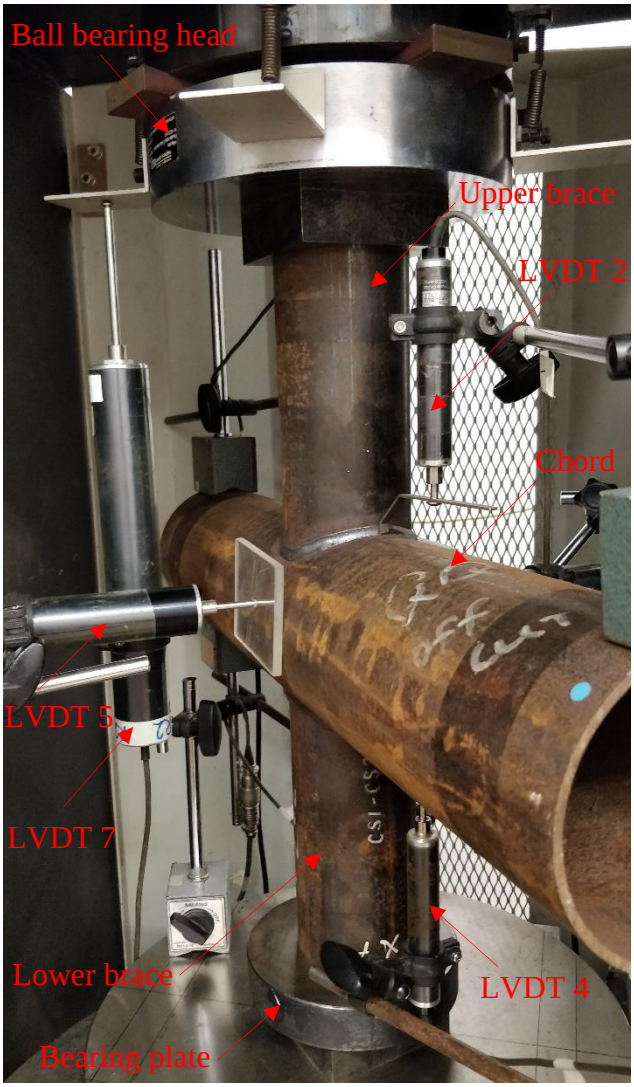

Fig. 4: Photo of setup for CFHSS CHS X-joint specimen 89×4*-108×4

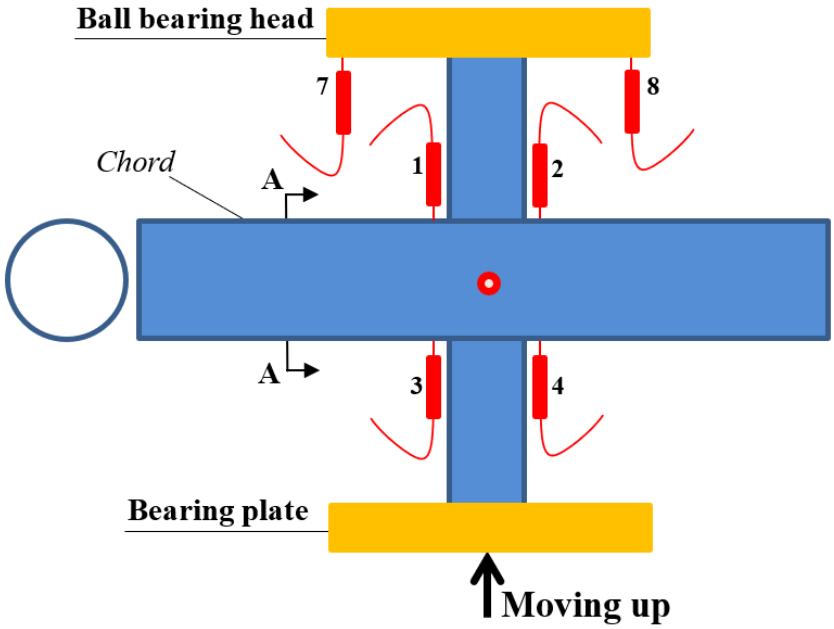

(a) Elevation view of X-joint set up

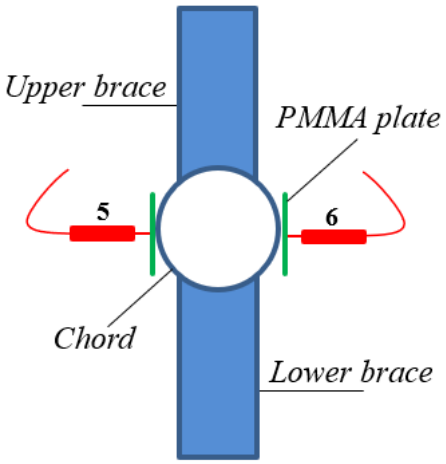

(b) Details of Section A-A

Fig. 5: Schematic view of test setup for CFHSS CHS X-joint

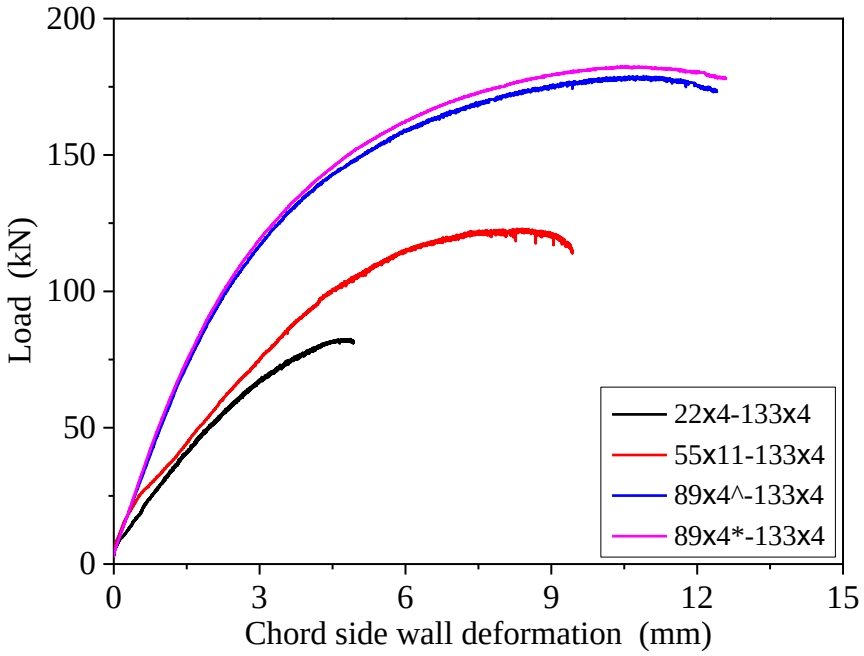

(a) Load-chord side wall deformation curves

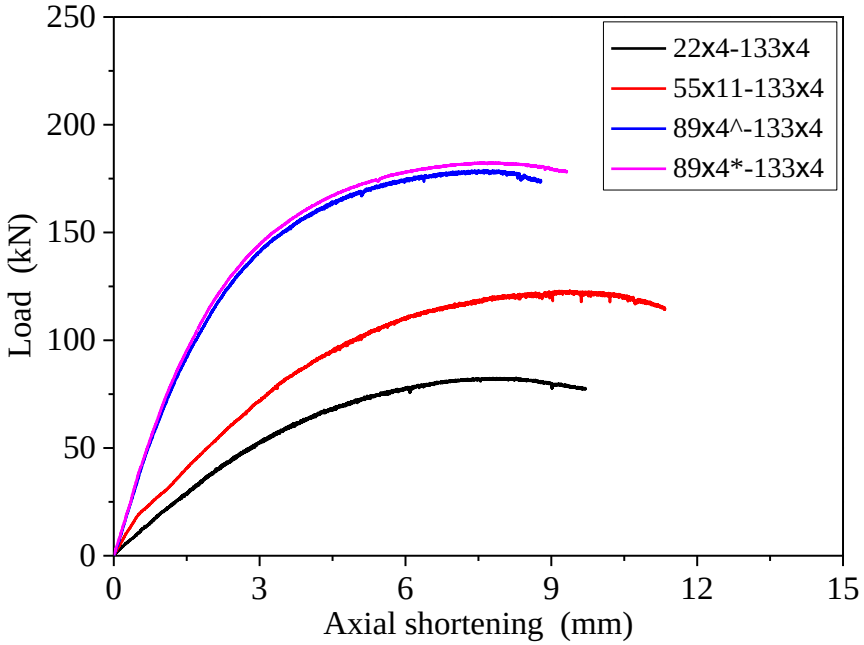

(b) Load-axial shortening curves at one side

Fig. 6: Test curves of X-joints with chord of 133×4 mm

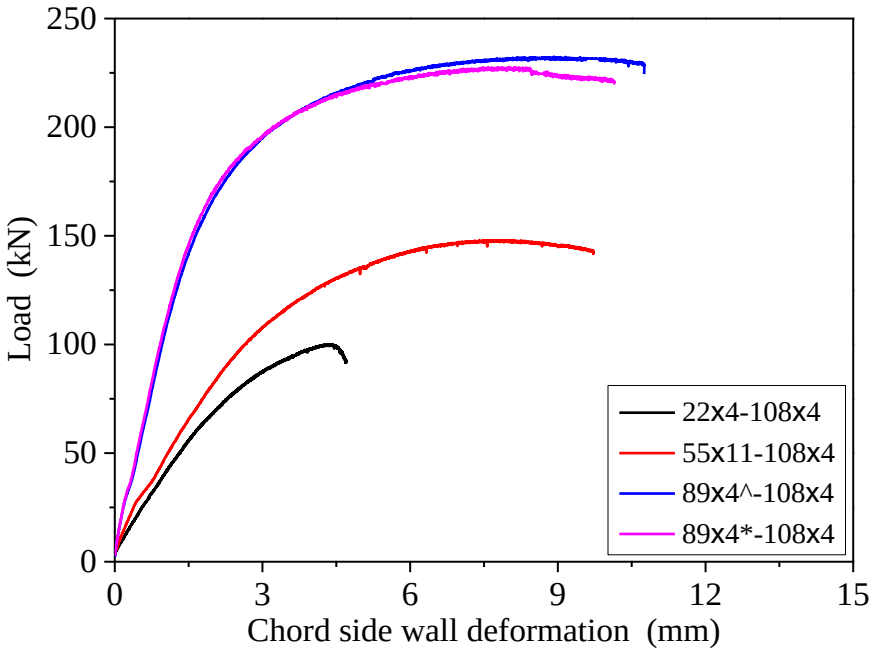

(a) Load-chord side wall deformation curves

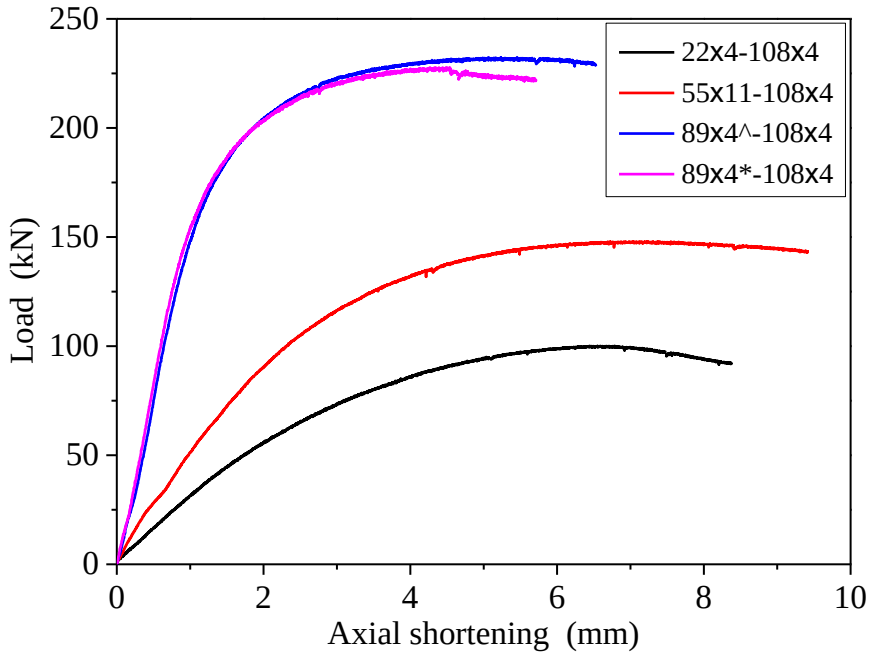

(b) Load-axial shortening curves at one side

Fig. 7: Test curves of X-joints with chord of 108×4 mm

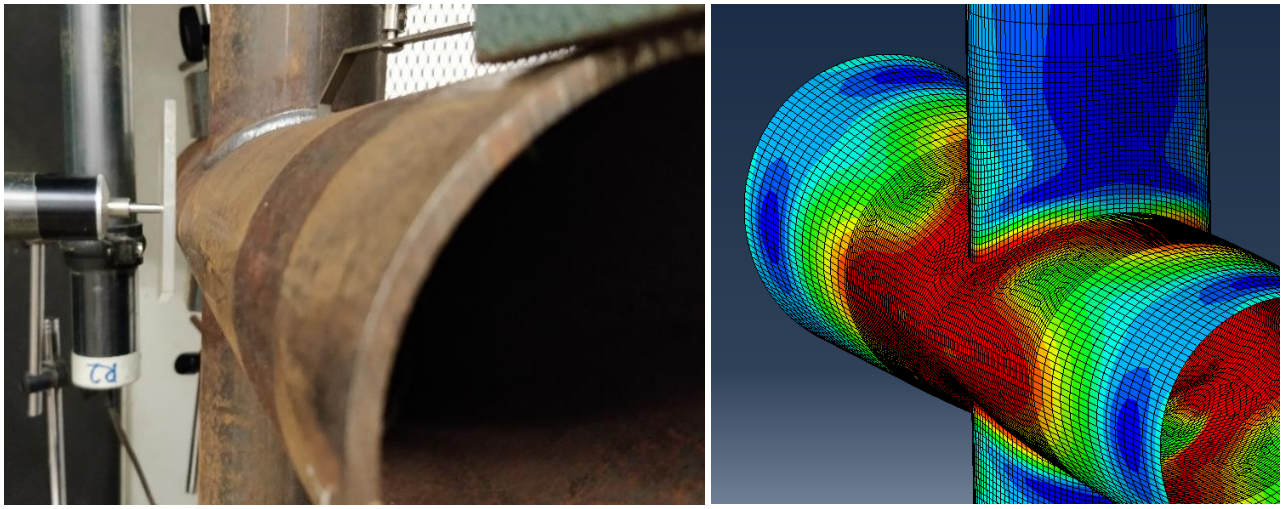

(a) Failure mode between test and FE results

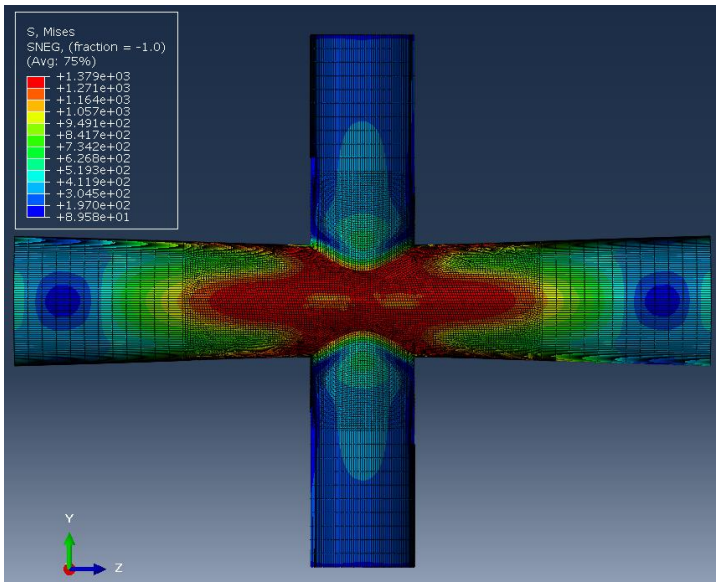

(b) Side view of FE result

Fig. 8: Failure mode comparison between test and FE results for specimen 89×4^-108×4

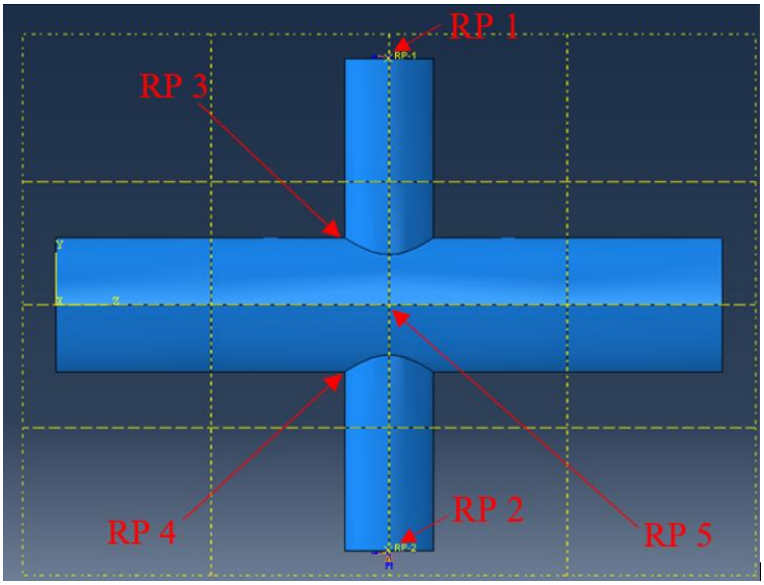

Fig. 9: Finite element model of CFHSS X-joint specimen 55×11 - 89×4*

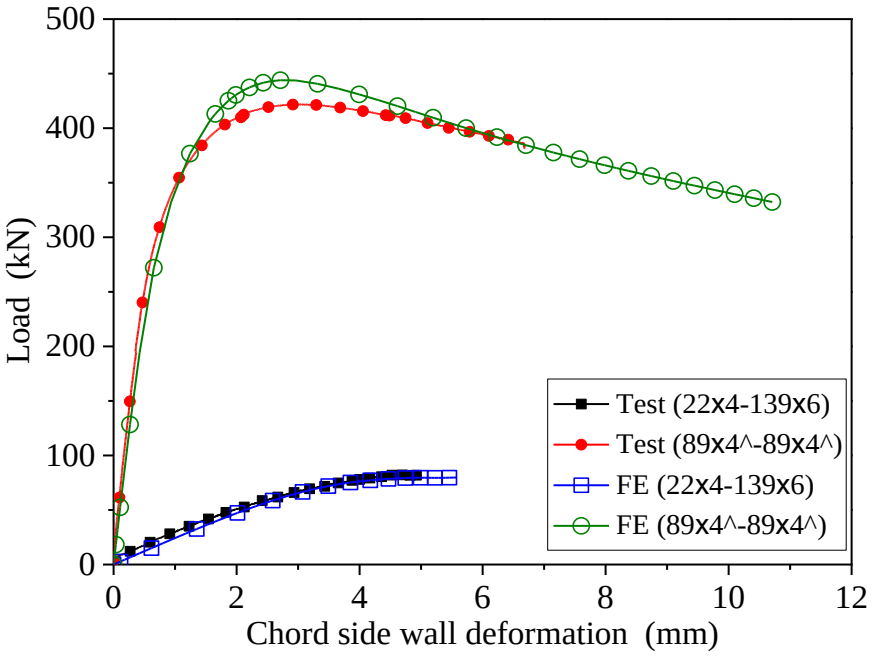

(a) Comparison of load-chord side wall deformation curves

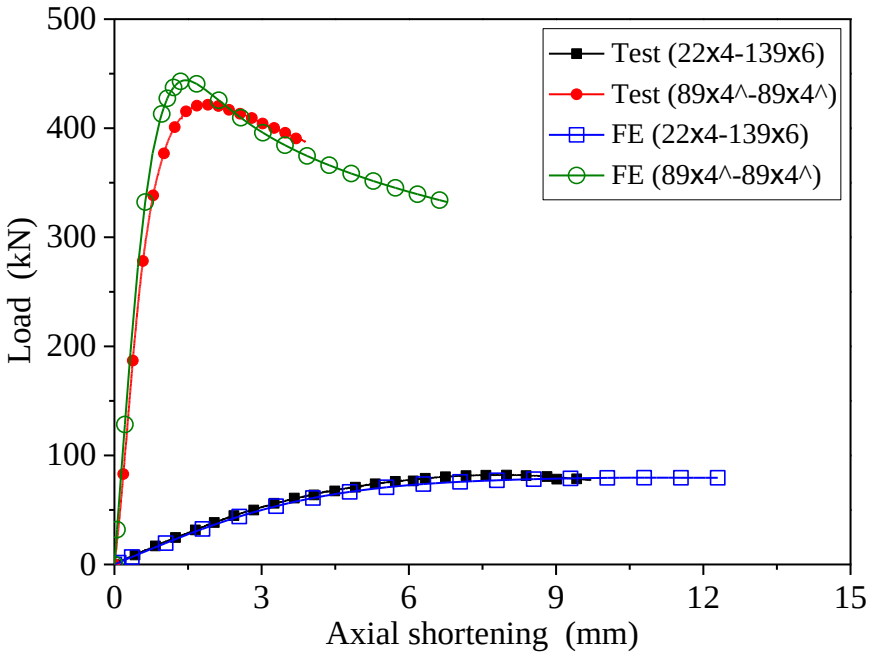

(b) Comparison of load-axial shortening curves at one side

Fig. 10: Comparison of load-deformation curves between test and FE results

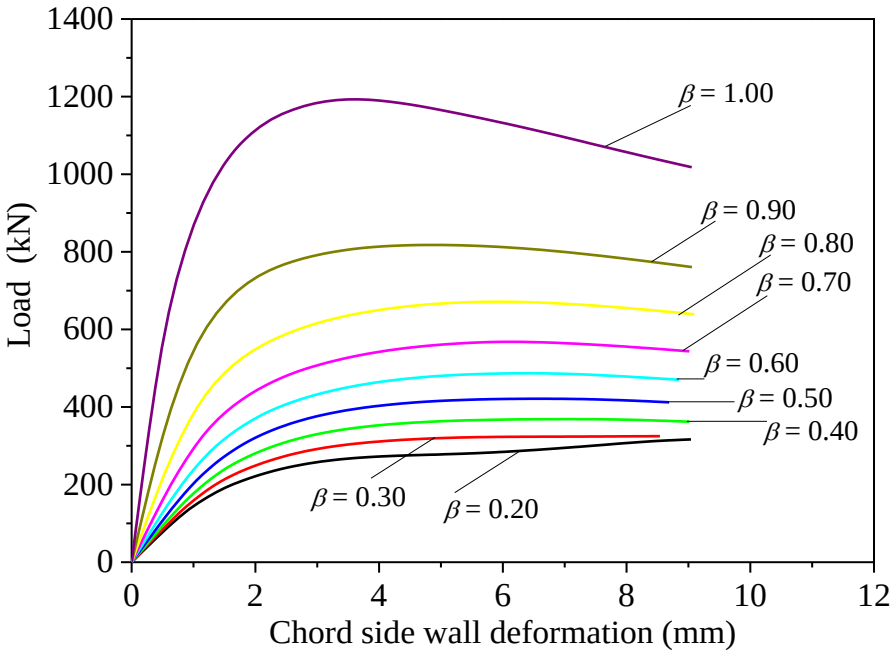

(a) Load-chord side wall deformation curves

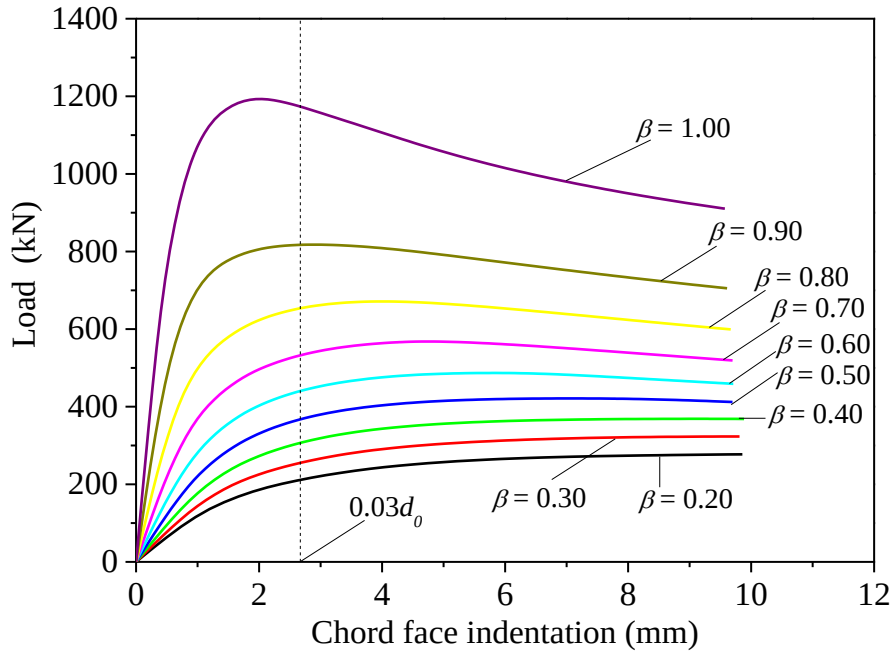

(b) Load-chord face indentation curves

Fig. 11: Curves of Series A with $\tau = 1.00$ and $2\gamma = 14.11$

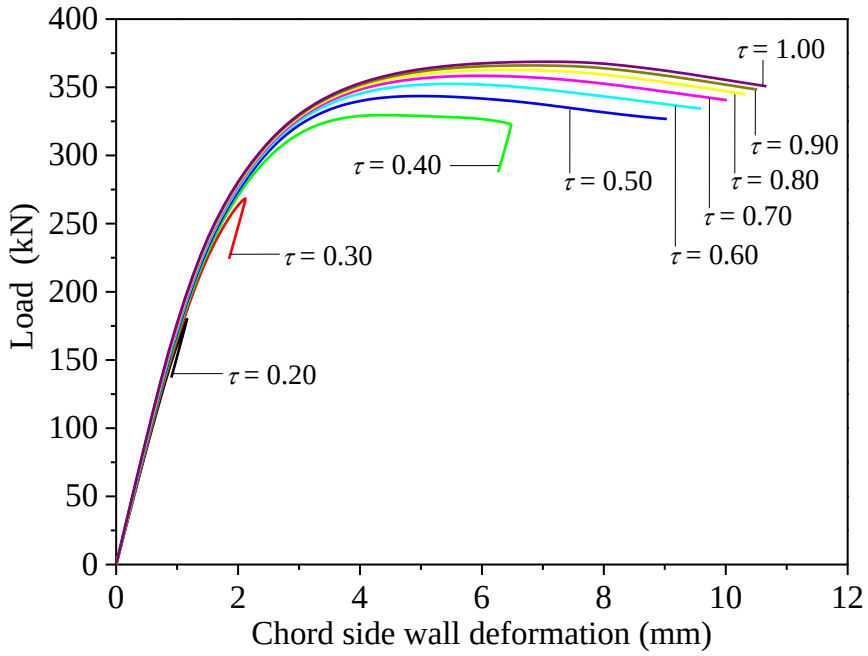

(a) Load-chord side wall deformation curves

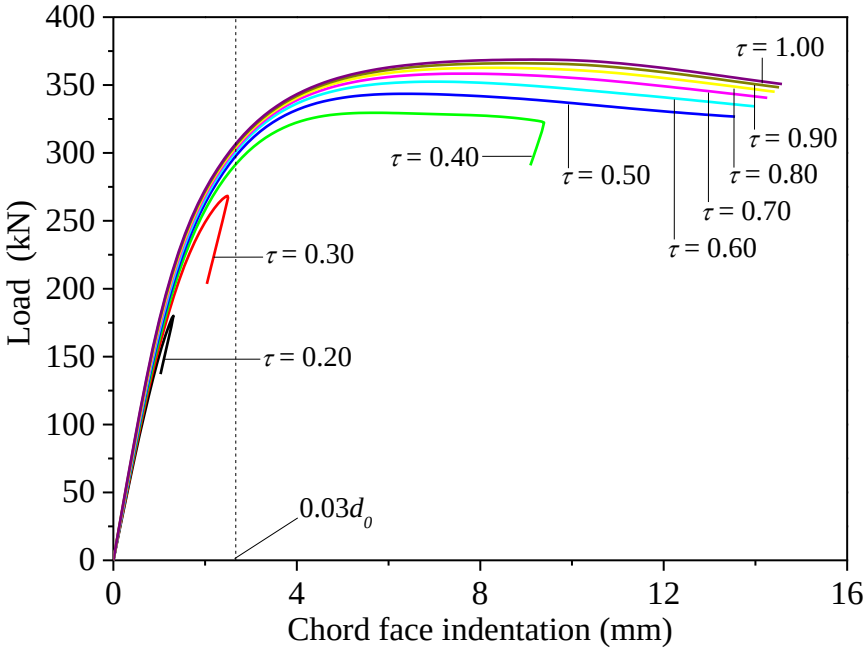

(b) Load-chord face indentation curves

Fig. 12: Curves of Series A with $\beta = 1.00$ and $2\gamma = 14.11$

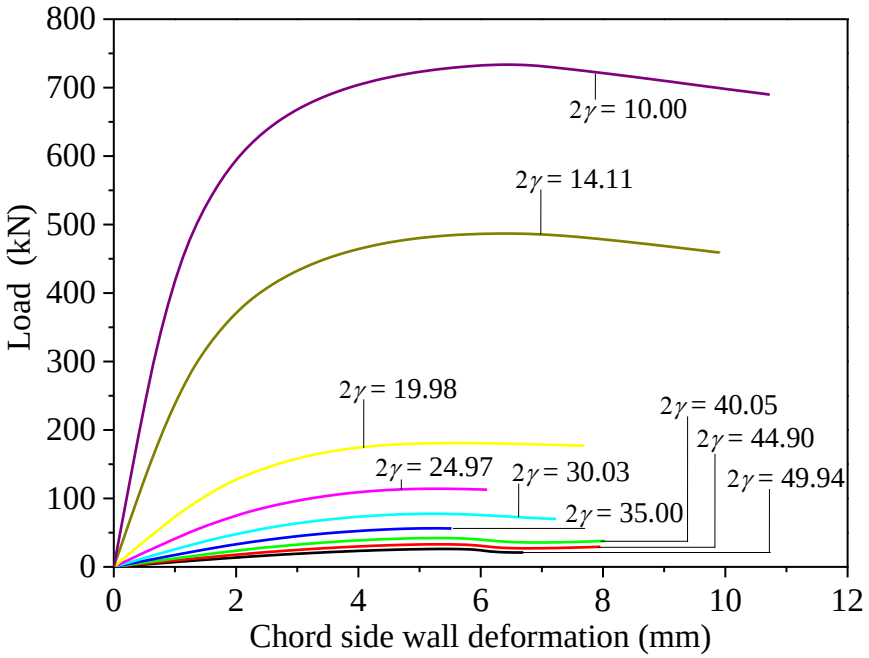

(a) Load-chord side wall deformation curves

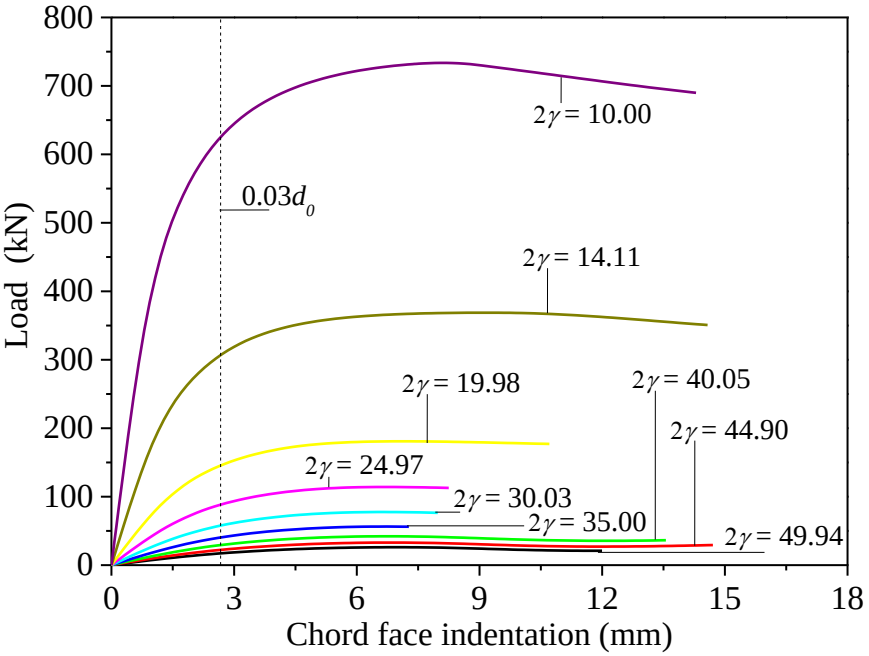

(b) Load-chord face indentation curves

Fig. 13: Curves of Series A with β = 1.00 and τ = 1.00

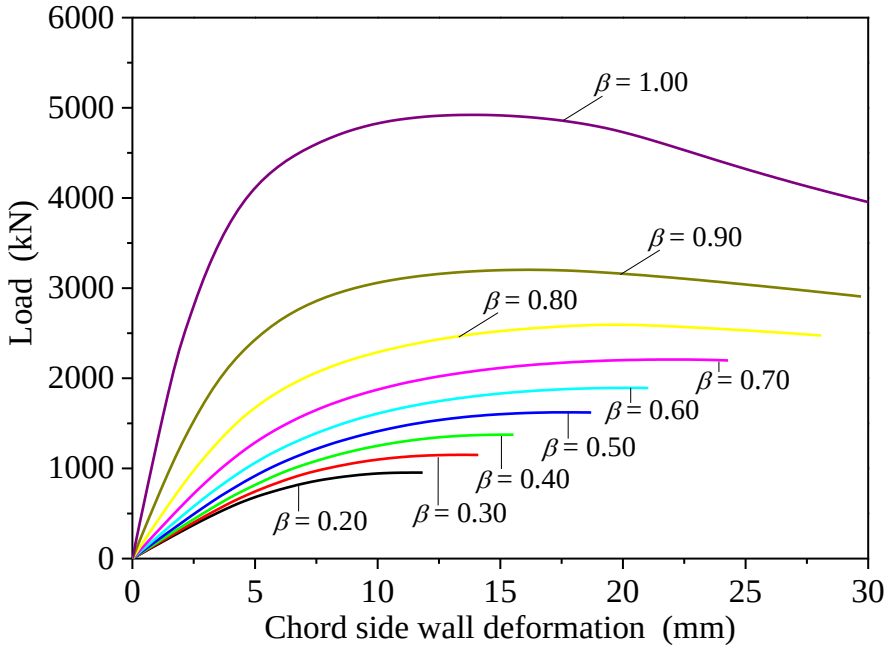

(a) Load-chord side wall deformation curves

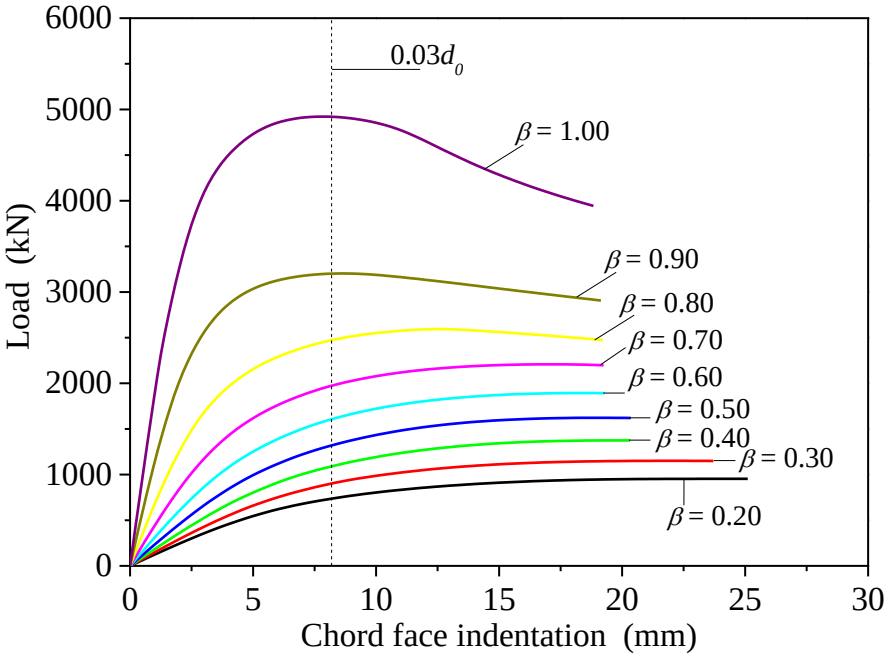

(b) Load-chord face indentation curves

Fig. 14: Curves of Series B with $\tau = 0.60$ and $2\gamma = 21.84$

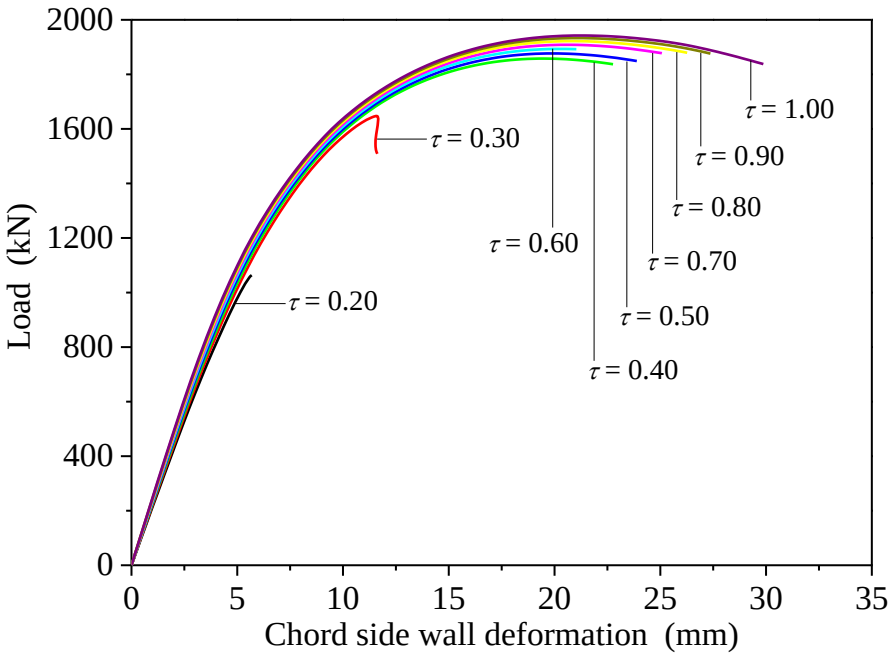

(a) Load-chord side wall deformation curves

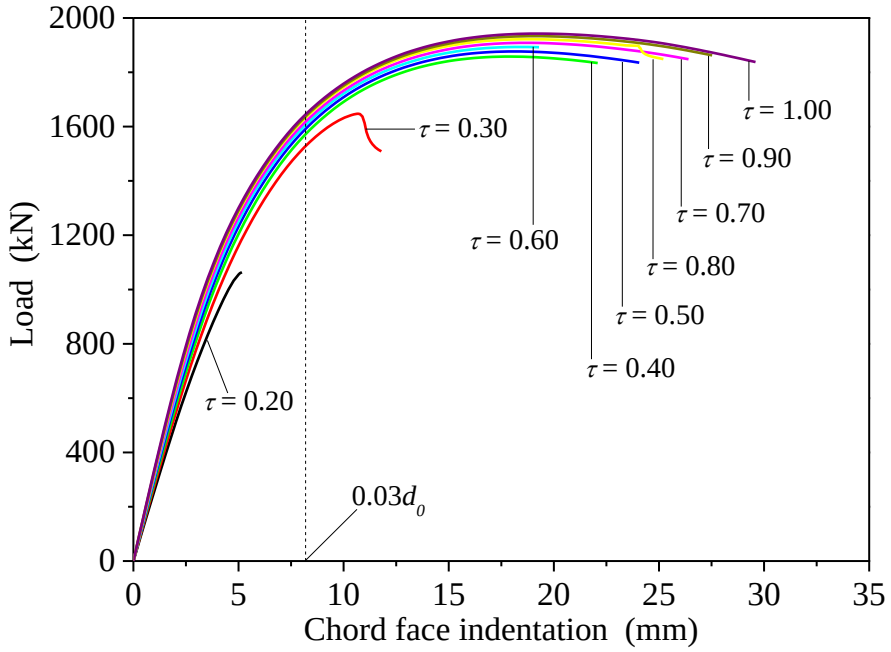

(b) Load-chord face indentation curves

Fig. 15: Curves of Series B with $\beta = 0.60$ and $2\gamma = 21.84$

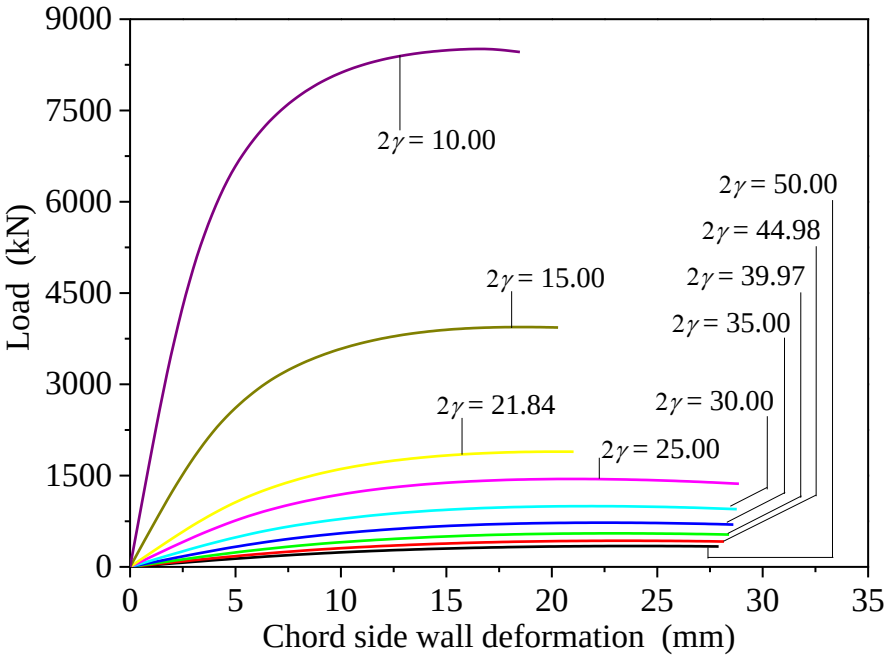

(a) Load-chord side wall deformation curves

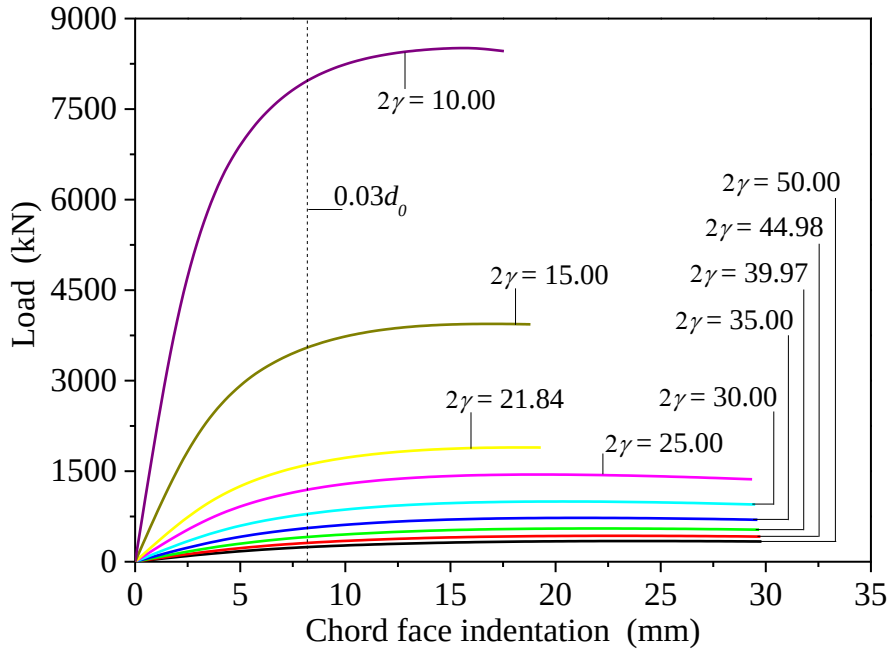

(b) Load-chord face indentation curves

Fig. 16: Curves of Series B with β = 0.60 and τ = 0.60

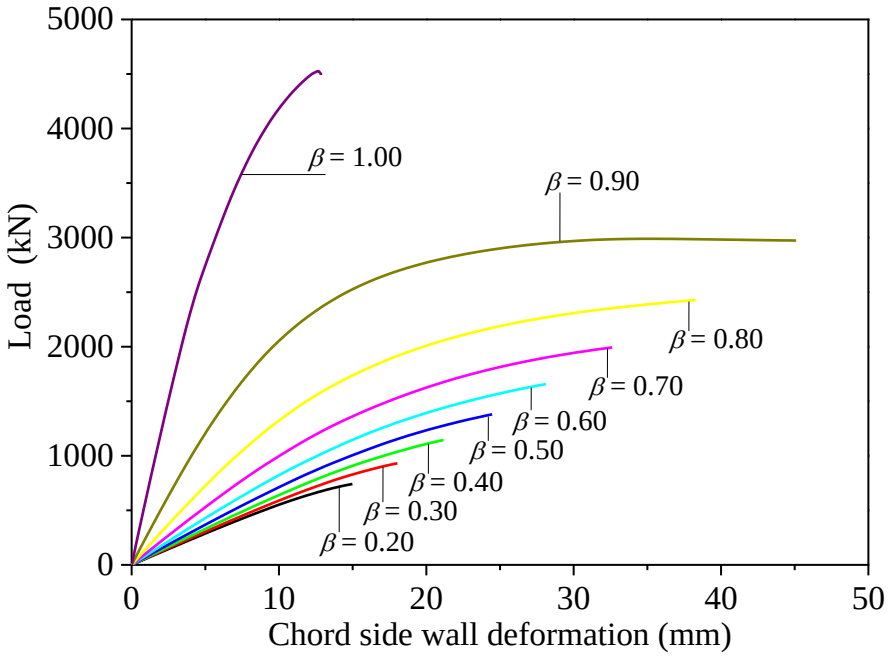

(a) Load-chord side wall deformation curves

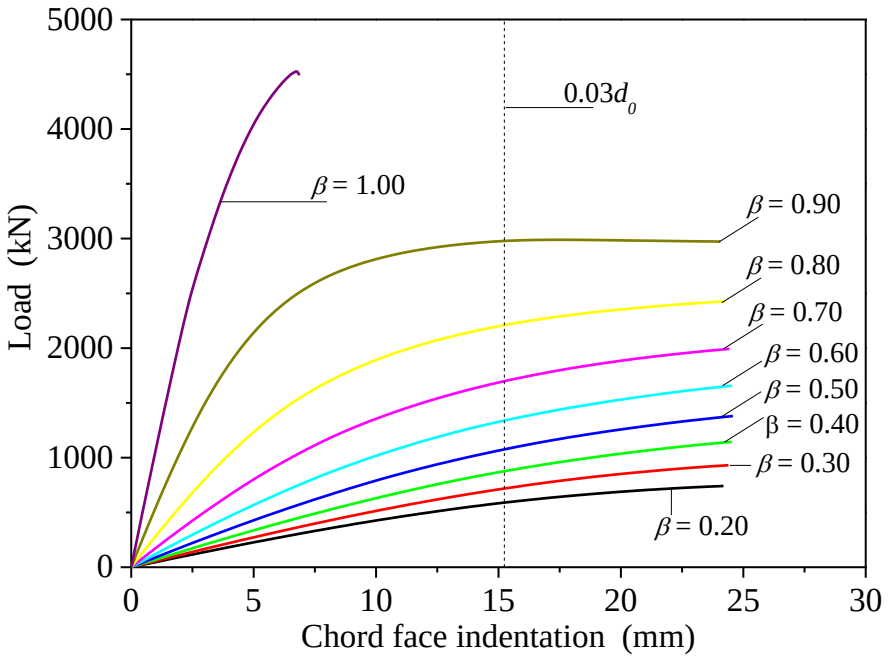

(b) Load-chord face indentation curves

Fig. 17: Curves of Series C with $\tau = 0.40$ and $2\gamma = 40.64$

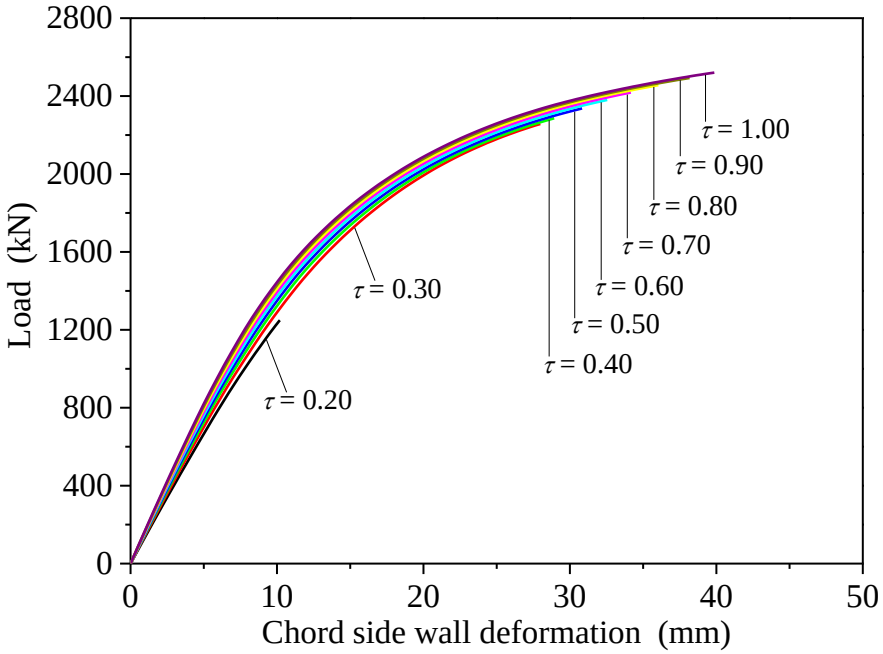

(a) Load-chord side wall deformation curves

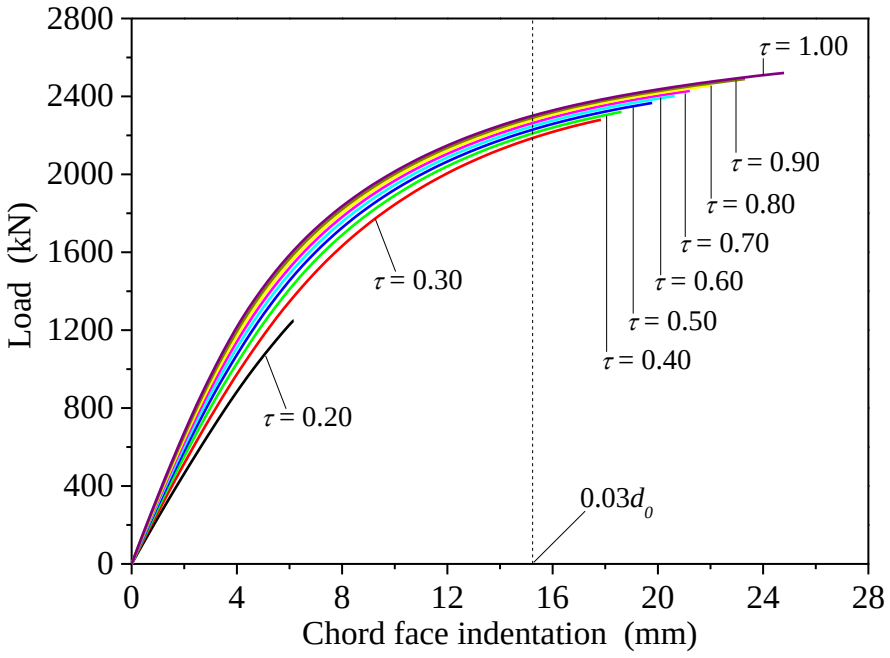

(b) Load-chord face indentation curves

Fig. 18: Curves of Series C with $\beta = 0.80$ and $2\gamma = 40.64$

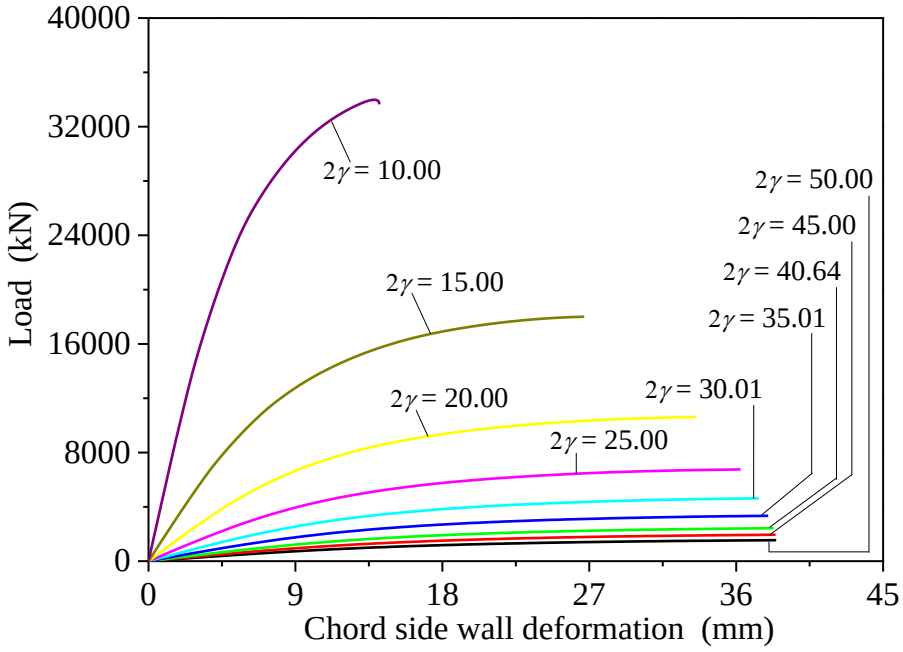

(a) Load-chord side wall deformation curves

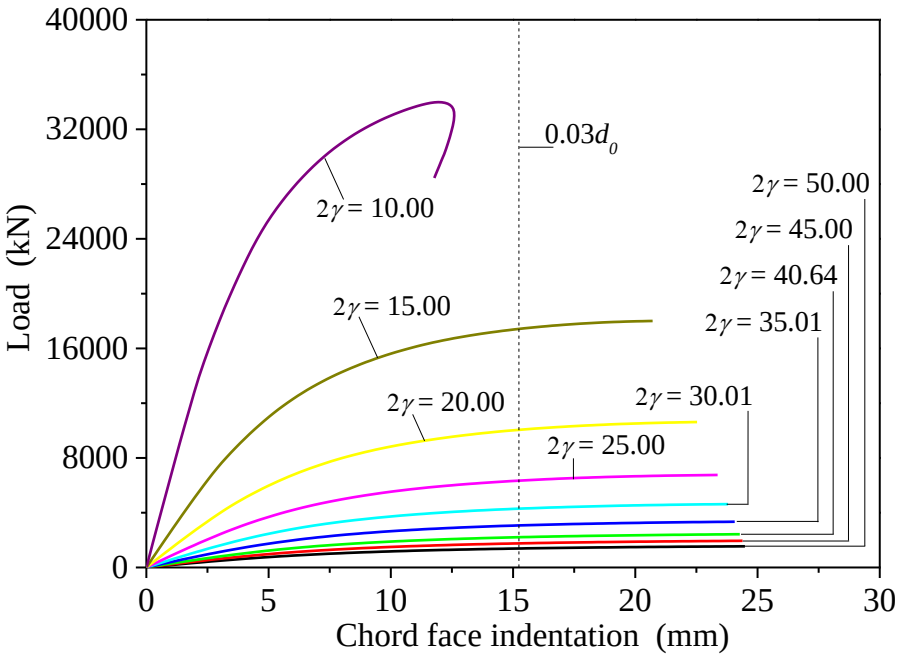

(b) Load-chord face indentation curves

Fig. 19: Curves of Series C with β = 0.80 and τ = 0.40

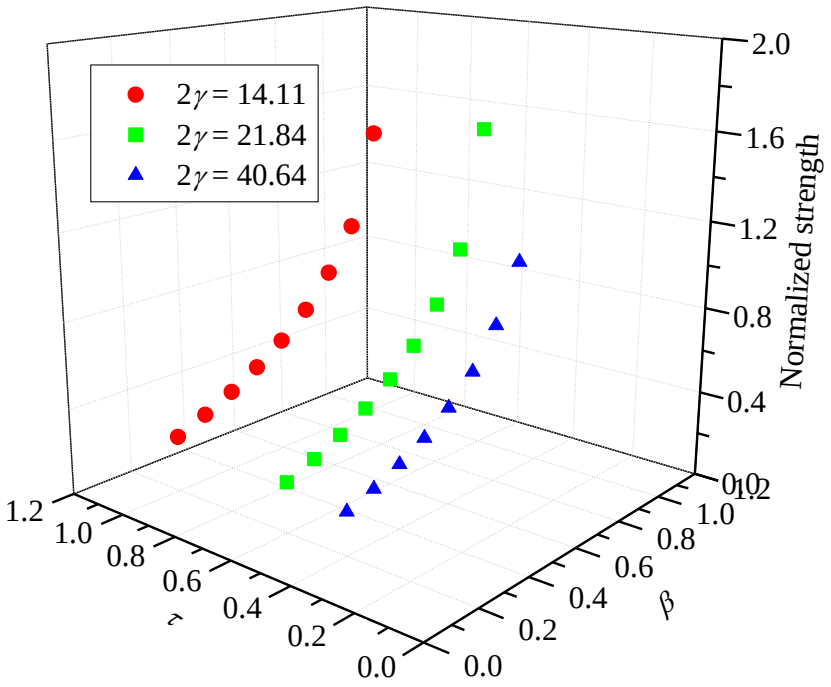

Fig. 20: Effects of β on the CFHSS circular tubular X-joint strengths

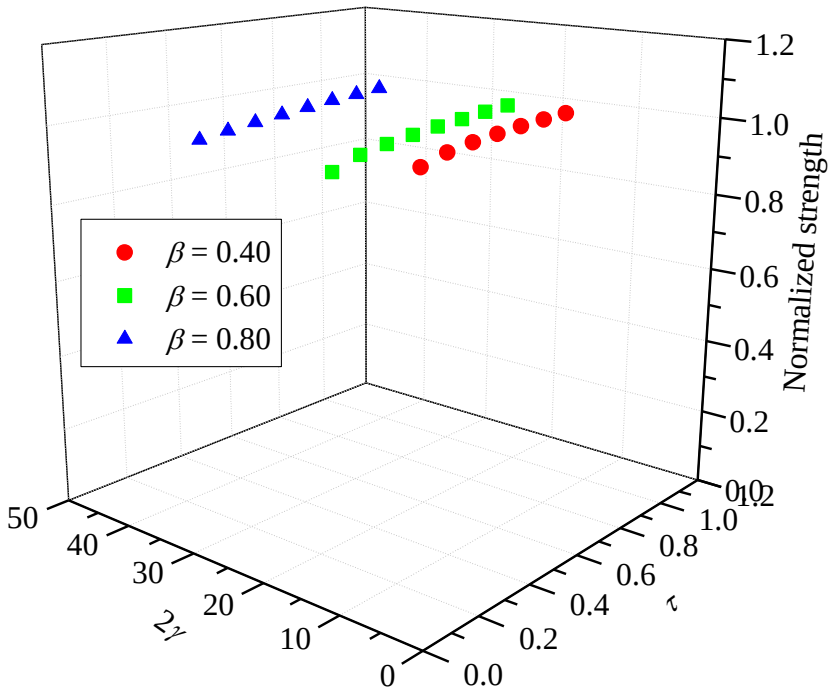

Fig. 21: Effects of τ on the CFHSS CHS X-joint strengths

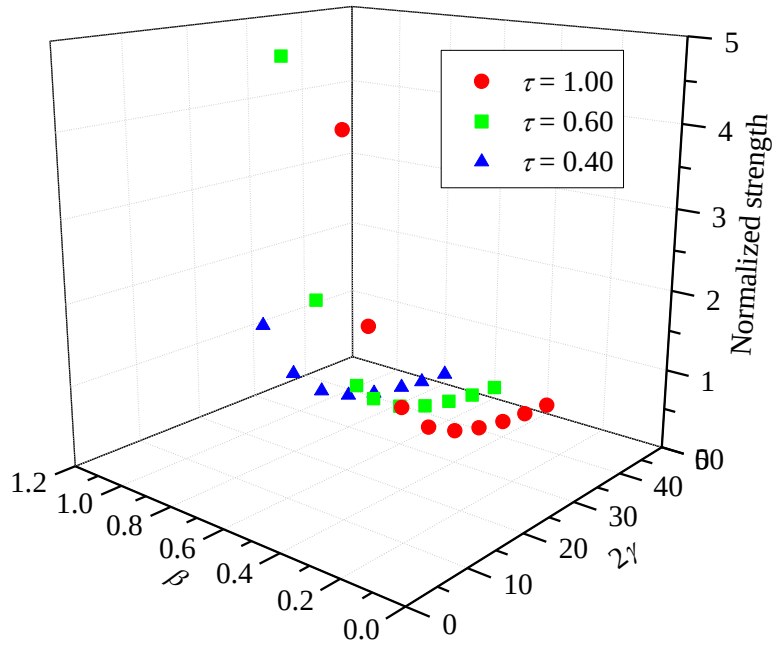

Fig. 22: Effects of 2γ on the CFHSS CHS X-joint strengths

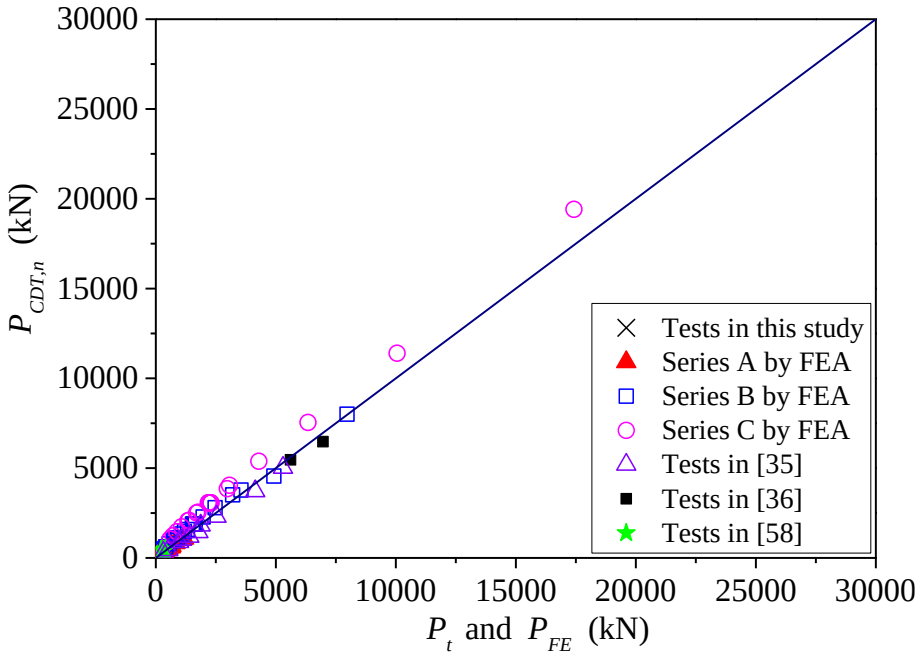

(a) Overall comparisons

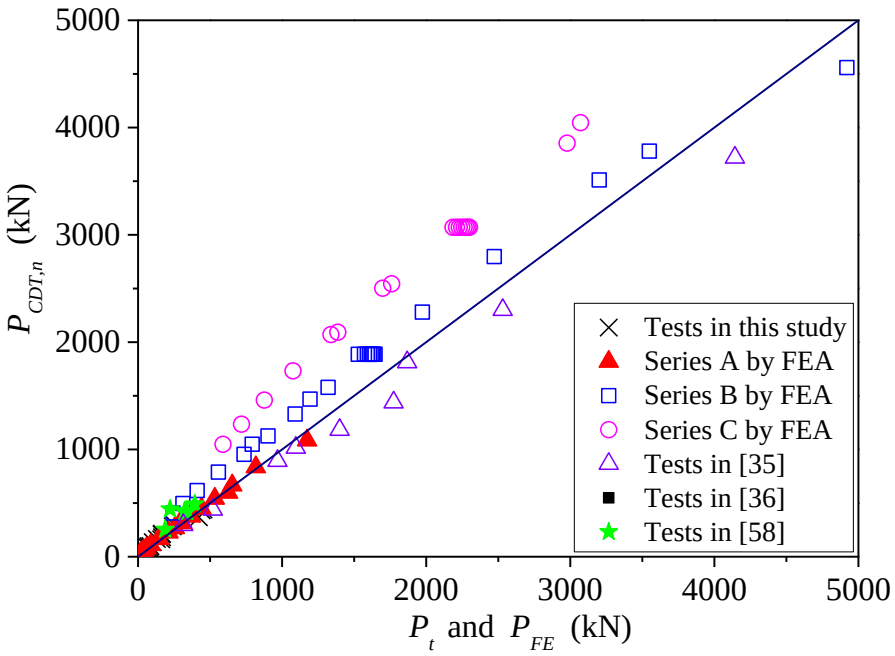

(b) Plot up to 5000 kN

Fig. 23: Comparison of test and FE strengths with predictions by CIDECT [52]

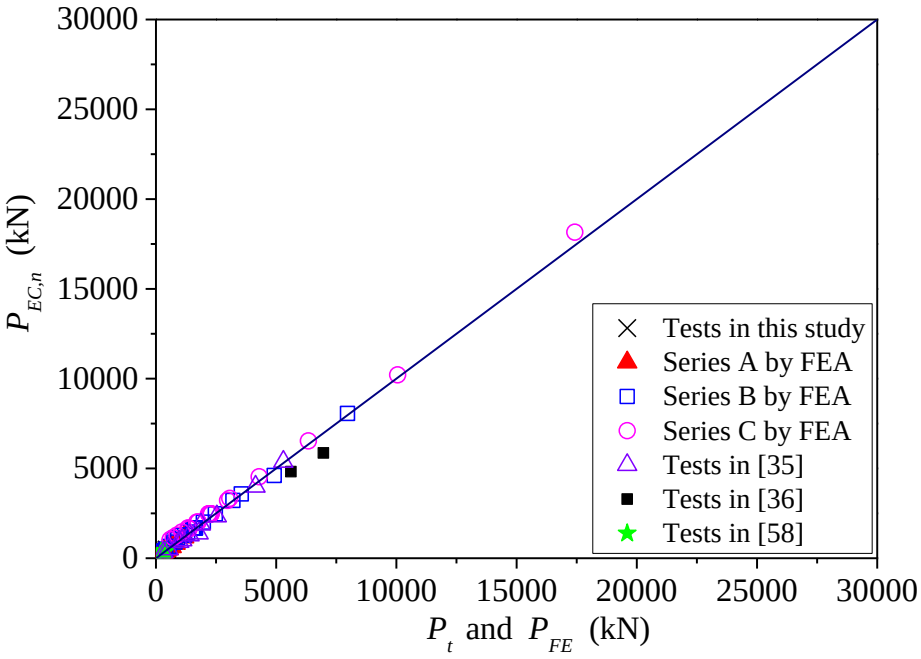

(a) Overall comparisons

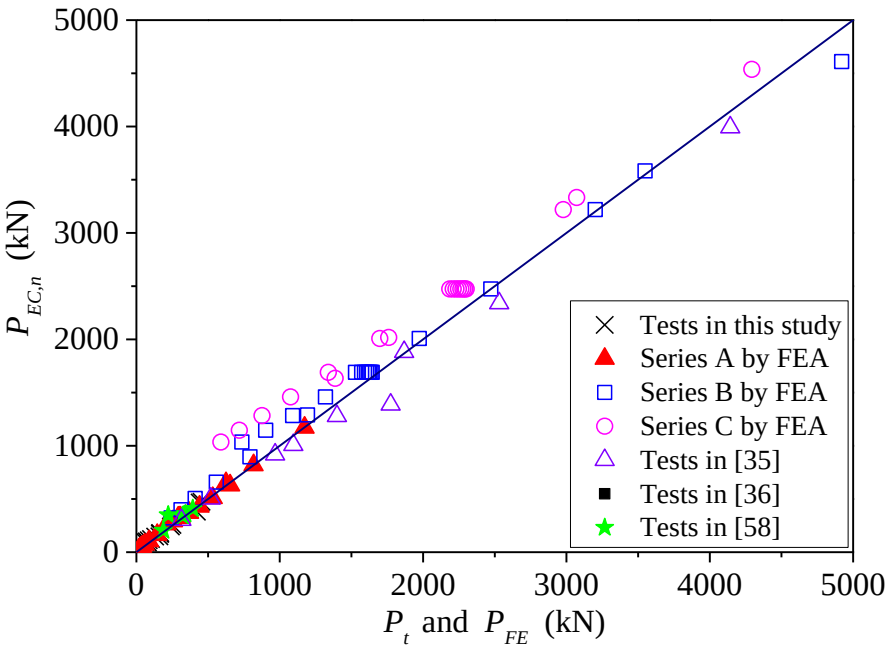

(b) Plot up to 5000 kN

Fig. 24: Comparison of test and FE strengths with predictions by EN-1993-1-8 [55]

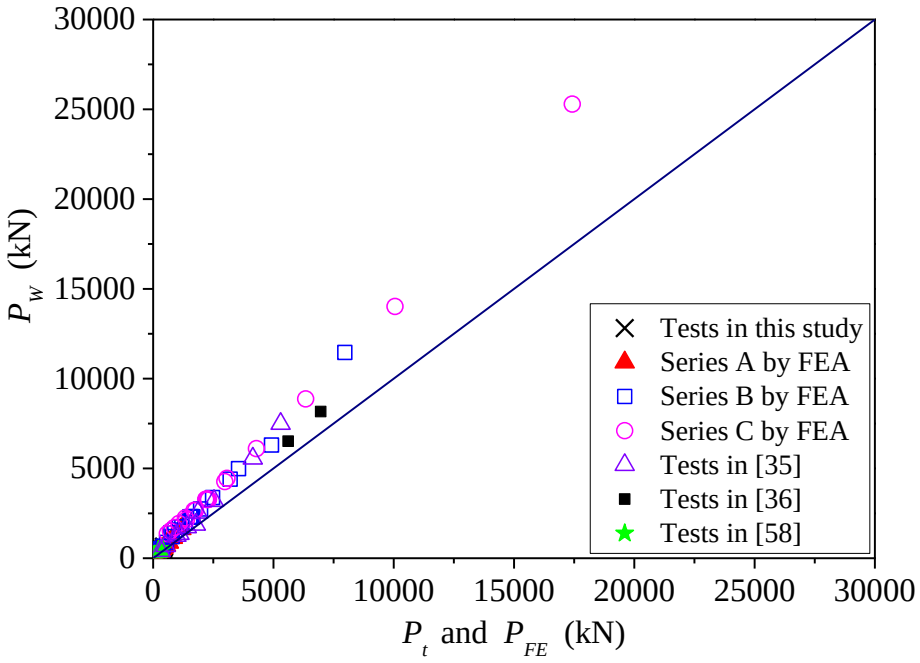

(a) Overall comparisons

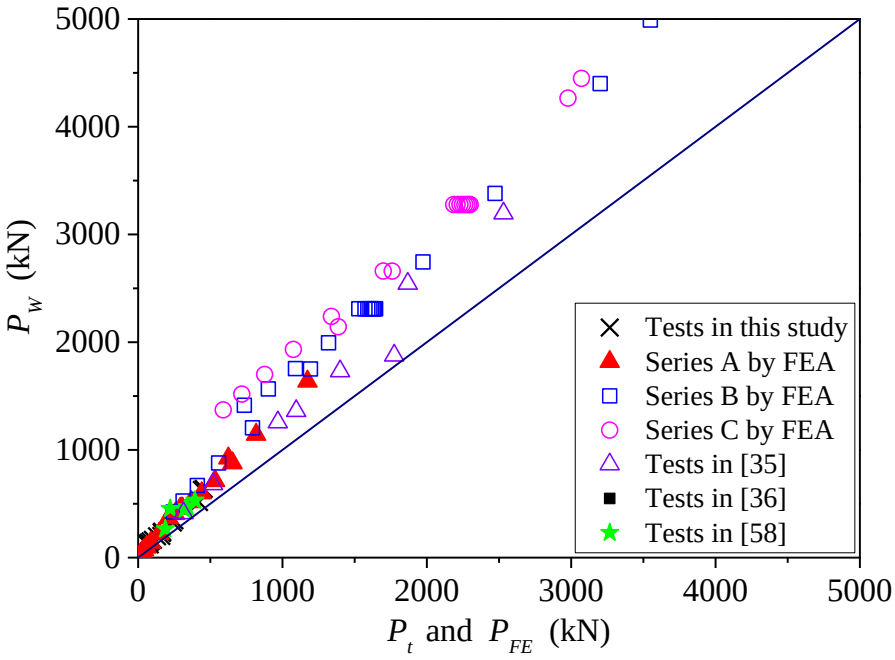

(b) Plot up to 5000 kN

Fig. 25: Comparison of test and FE strengths with predictions Wardenier [66]

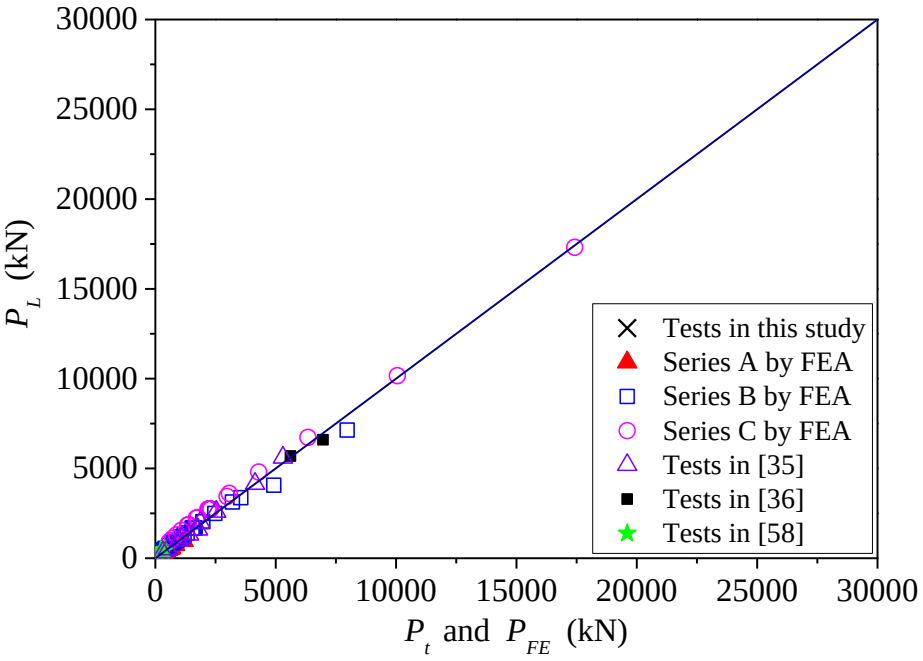

(a) Overall comparisons

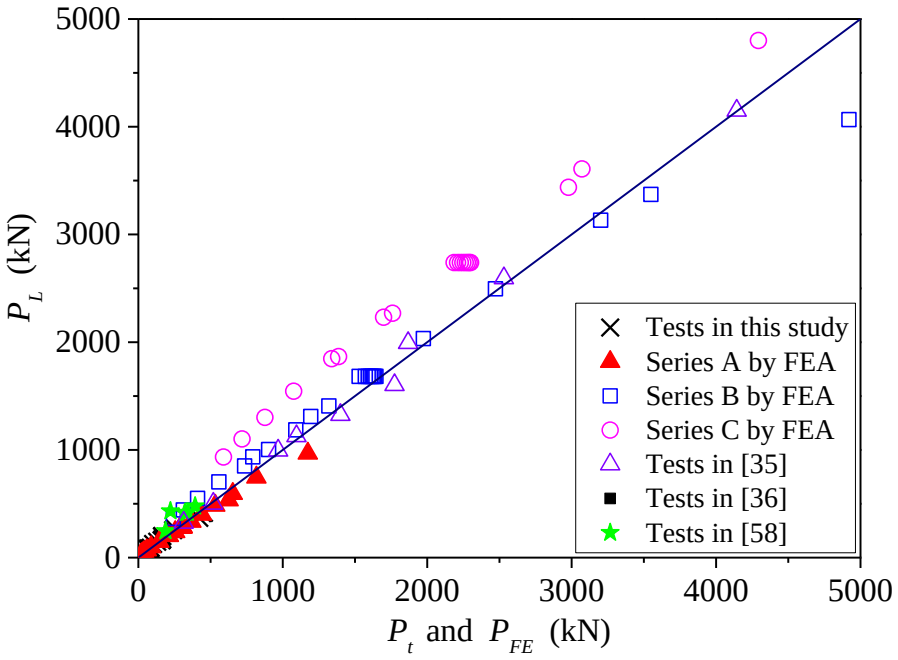

(b) Plot up to 5000 kN

Fig. 26: Comparison of test and FE strengths with predictions by Lan *et al.* [38]

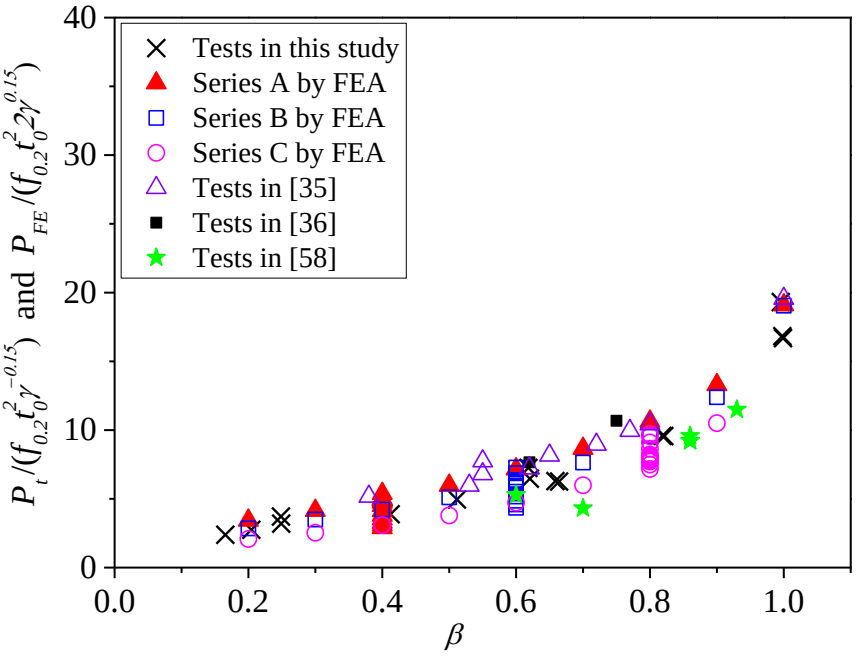

Fig. 27: Relationship between joint strengths divided by ($f_{0.2}t_0^2\gamma^{0.15}$) and β

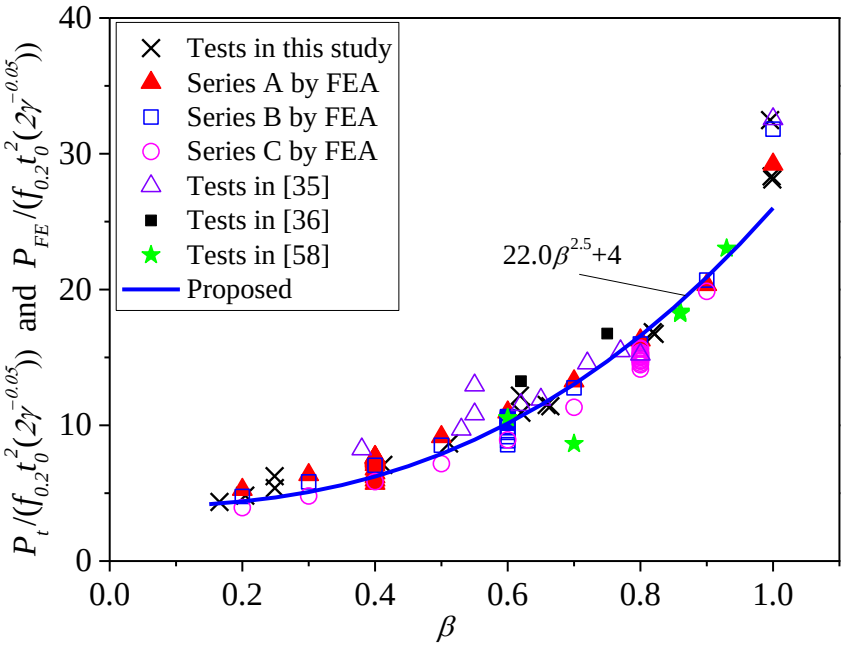

Fig. 28: Relationship between joint strengths divided by ($f_{0.2}t_0^2(2\gamma^{-0.05})$) and β

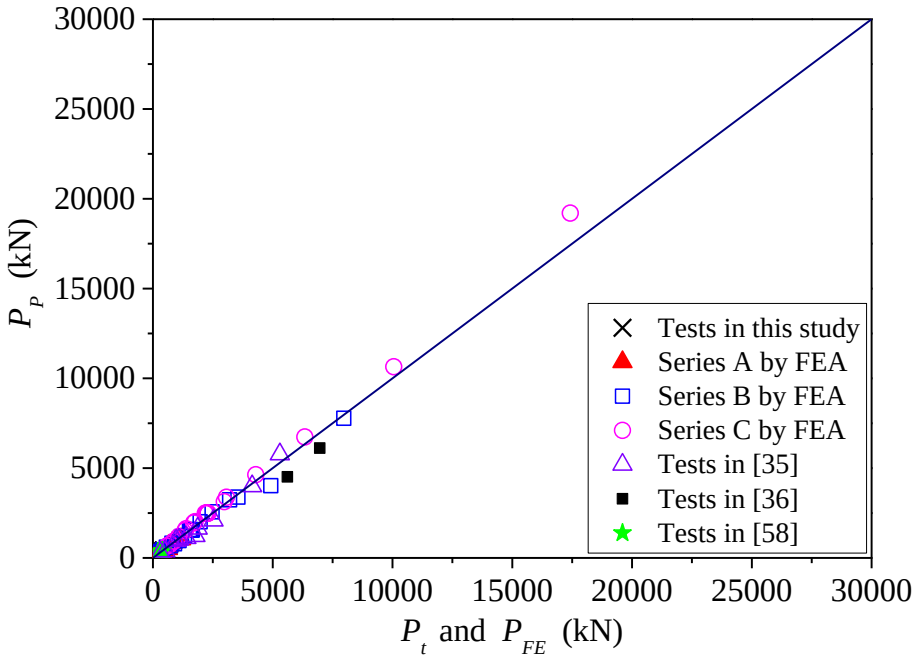

(a) Overall comparisons

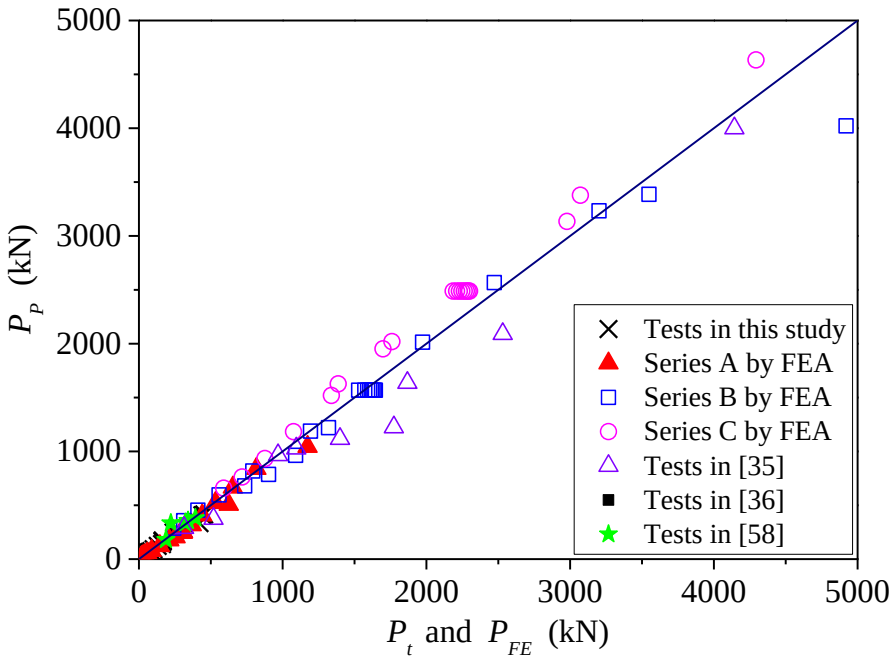

(b) Scale up to 5000 kN

Fig. 29: Comparison of test and FE strengths with predictions by proposed equation